J. Fluid Mech. (1997), *vol.* 349, *pp.* 295–325. Printed in the United Kingdom

Subharmonic resonance of Venice gates in waves. Part 1. Evolution equation and uniform incident waves

By PAOLO SAMMARCO†, HOANG H. TRAN AND CHIANG C. MEI

Parsons Laboratory, Department of Civil and Environmental Engineering, Massachusetts Institute of Technology, Cambridge, MA 02139, USA

(Received 7 February 1997 and in revised form 17 June 1997)

For flood protection against storm tides, barriers of box-like gates hinged along a bottom axis have been designed to span the three inlets of the Venice Lagoon. While on calm days the gates are ballasted to rest horizontally on the seabed, in stormy weather they are raised by buoyancy to act as a dam which is expected to swing to and fro in unison in response to the normally incident sea waves. Previous laboratory experiments with sinusoidal waves have revealed however that neighbouring gates oscillate out of phase, at one half the wave frequency, in a variety of ways, and hence would reduce the effectiveness of the barrier. Extending the linear theory of trapped waves by Mei *et al.* (1994), we present here a nonlinear theory for subharmonic resonance of mobile gates allowed to oscillate about a vertical plane of symmetry. In this part (1) the evolution equation of the Landau–Stuart type is first derived for the gate amplitude. The effects of gate geometries on the coefficients in the equation are examined. After accounting for dissipation effects semi-empirically the theoretical results on the equilibrium amplitude excited by uniform incident waves are compared with laboratory experiments.

1. Introduction

For reducing the hazards of flooding in Venice, storm barriers have been designed to span the three inlets of Venice Lagoon. The proposed barriers will consist of a series of hollow steel gates which are unconnected to each other but hinged at the bottom along a common axis on the seabed. In calm weather the gates rest horizontally on the seabed so as not to obstruct normal navigation or to impair the scenic view of the area. In stormy weather, all gates will be raised by filling the box-like gates with compressed air to an inclination of about 50° from the horizontal, and hence will act as a dam. The gates are otherwise free and are expected to swing to and fro in unison in normally incident waves and maintain the sea-level difference. Laboratory experiments with sinusoidal waves incident normally on two or three gates in a narrow flume, or on a large number of gates in a wide basin, have however revealed that neighbouring gates may oscillate out of phase in a variety of ways, at half of the frequency and with relatively large amplitude (Consorzio Venezia Nuova, 1988*a*, *b*; Varisco 1992). The out-of-phase motion must be understood in order to take proper measures for preserving the intended efficiency of the gates as a dam.

† Present address: DITS, University of Rome 'La Sapienza', Italy.

It is known that edge waves which are natural modes trapped on a sloping beach can be resonated subharmonically by incident waves (Guza & Bowen 1976; Minzoni & Whitham 1976; Rockliff 1978; Miles 1990). Mei *et al.* (1994) showed that articulated gates of finite dimensions hinged at the bottom can also support trapped waves even if they are upright in the state of static equilibrium. They deduced a linearized theory for the eigenmodes, and performed confirming experiments for the simplest mode sketched in figure 1. Furthermore they have given experimental evidence that the gate resonance is indeed associated with these trapped modes and anticipated that the nonlinear dynamics should also be governed by the Stuart–Landau equation.

A simplified linear theory of trapped modes near articulated gates has been independently developed by Blondeaux, Seminara & Vittori (1993*a*, *b*) who considered vertical slices sliding horizontally on the sea bottom. Other simplifying assumptions are: (i) the thickness of a slice in the direction along the barrier axis (i.e. across the inlet) is so small that there is negligible transverse rigidity; (ii) buoyancy of the hollow gates is represented by a fictitious linear spring, and (iii) waves are assumed to be very long compared to the water depth. The properties of the trapped modes are found as functions of the channel dimensions, the mass of the gate, and the stiffness of the artificial linear spring (Blondeaux *et al.* 1993*a*). When the gates are forced by plane incident waves the threshold of instability of these modes is found to be governed by a Mathieu equation (Blondeaux *et al.* 1993*b*). Recently, Vittori, Blondeau & Seminara (1996) have further extended this simple model to include nonlinearity. Energy is lost only through radiation damping, similar to the edge-waves theory of Rockliff (1978). Equilibrium solutions and their bifurcations and instability are discussed.

In real fluids viscous damping must exist in addition to radiation damping. For the edge-wave problem, Miles (1990) has modelled the effects of viscosity by a linear dissipation term, and found a critical incident amplitude below which the edge wave cannot be resonated. Buchan & Pritchard (1995) have conducted detailed experiments for edge waves. The threshold of instability, the growth rate and resonance amplitude are measured for different incident wave amplitude and frequency. In comparison, the theoretical threshold of Miles is shifted somewhat to the left of the observed data, i.e. towards negative detuning. The experimental threshold curve displays two local maxima along the frequency axis, which are not predicted by the theory and are attributed to the interaction between the edge wave and a long-period seiche in the wave channel.

The mechanism of Faraday resonance (subharmonic resonance of cross-waves by a monolithic piston)† in a basin is partially similar, with viscosity being the primary source of dissipation. Hendersen & Miles (1991) have shown that the response diagram in the plane of oscillation amplitude vs. forcing frequency contains the characteristics of hysteresis and jump phenomena. These features and the instability threshold are also verified experimentally (Hendersen & Miles, 1991). Recent work by Jiang *et al.* (1996) further confirmed the nonlinear state which exhibits hysteresis in the response plane of amplitude vs. frequency.

In this two-part paper, we describe a weakly nonlinear theory of the mobile-gate dynamics, by both theory and experiment, based on the more realistic geometry of Mei *et al.* (1994). We first derive in Part 1 the anticipated evolution equation. The dependence

† Jongeling & Kolkman (1995) suggested that the Faraday resonance is responsible for the out-of-phase oscillation of the gates. Experiments by Mei *et al.* (1994) showed this not to be the case since cross-channel variations diminish quickly away from the gates. Cross-waves are caused by, and can only coexist with, gates oscillating in phase at the same order of magnitude. Thus the articulateness of the gates is the active cause of the phenomenon under study, rather than the passive response.

of all coupling coefficients on the gate characteristics will be examined. The effects of steady incident waves will then be studied. Laboratory experiments are performed to compare with theoretical predictions. For best corroboration between theory and experiment two viscous damping terms are found to be necessary, one linear for lower amplitudes and one quadratic for higher amplitudes. The coefficients of these damping terms are determined empirically from free oscillation tests without incident waves. With incident waves the predicted hysteresis and jump phenomenon are verified.

In Part 2 (Sammarco *et al.* 1997) we shall extend the theory for sinusoidally modulated incident waves, as the simplest model of a narrow-banded sea spectrum. Because the gate envelope is now governed by a non-autonomous dynamical system, various bifurcations corresponding to modulational resonances occur. Extensive experiments are performed to check the theoretical predictions of modulational bifurcations and chaos.

2. Order estimates

As in the edge-wave problem (Minzoni & Whitham 1976; Rockliff 1978), we first assume that a trapped mode will be resonated, and estimate the time scale of resonant growth, the amplitude of the trapped waves in the nonlinear stage, as well as the amplitude of the forcing incident waves.

Let the angular displacement of the gate associated with the trapped wave motion be denoted by Θ^T

$$\Theta^T = \theta^T \mathrm{e}^{-\mathrm{i}\omega_0 t} + *, \tag{2.1}$$

where ω_0 is the eigenfrequency, and $*$ signifies the complex conjugate of the preceding term. Let the angular displacement of the gate forced by an incident plane wave of amplitude A be

$$\Theta^A = \theta^A \mathrm{e}^{-2\mathrm{i}\omega_0 t} + *. \tag{2.2}$$

Similar to the edge-wave problem, the equation coupling the motions of the gates and the waves is expected to be of the following symbolic form:

$$\mathscr{L}\Theta^T + \mathscr{L}\Theta^A = (\Theta^T, \Theta^A) + (\Theta^T, \Theta^T, \Theta^T) + (\Theta^T, \Theta^A, \Theta^A) + \ldots, \tag{2.3}$$

On the left-hand side the linear operator $\mathscr{L}$ is composed of inertia, buoyancy and linear dynamic pressure

$$\mathscr{L}\{\cdot\} = I\frac{\partial^2\{\cdot\}}{\partial t^2} + C\{\cdot\} - \rho\int_{-h}^{0} \mathrm{d}z\,(z+h)B\frac{\partial\{\cdot\}}{\partial t}, \tag{2.4}$$

where I denotes the rotational inertia of the gate and C the buoyancy restoring moment, B a proportionality factor relating the angular displacement of the gate and the velocity potential, and ρ the fluid density. On the right-hand side of (2.3), we have retained only those quadratic and cubic terms which will resonate the first harmonic $\pm\omega_0$; their orders of magnitudes are respectively

$$|\Theta^T||\Theta^A|, \qquad |\Theta^T|^3, \qquad |\Theta^T||\Theta^A|^2. \tag{2.5}$$

At the beginning of resonance $|\Theta^T| \ll |\Theta^A|$; the first term on the right of (2.5), representing forcing by the incident wave, is the most important. The amplitude $|\Theta^T|$ must increase slowly in time. From $I\Theta^T_{tt}$, the term dominating the initial growth must be proportional to $-\mathrm{i}\omega_0|\Theta^T_t|$. In order that the growth rate balances wave forcing, the time scale of resonance growth must be $\sim 1/\omega_0|\Theta^A|$. Consequently, two time scales are inherent in this problem: $1/\omega_0$ and $1/\omega_0|\Theta^A|$. At the mature state of resonance,

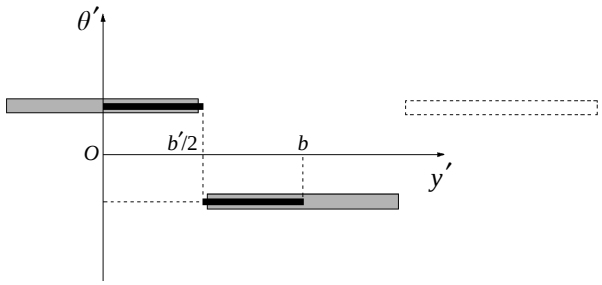

FIGURE 1. The simplest mode of oscillation for an array of gates.

equilibrium is attained. The cubic and quadratic nonlinearities are in balance, which is only possible when the first and second terms of (2.5) are of the same magnitude, $|\Theta^T||\Theta^A| \sim |\Theta^T|^3$, hence $|\Theta^T| \sim |\Theta^A|^{1/2}$.

In summary, if the amplitude of the trapped wave oscillating on a fast scale $1/\omega_0$ is scaled to be $O(1)$, then the incident wave must be $O(\epsilon)$, with $\epsilon \ll 1$ a small ordering parameter, and the time scale of growth will be $1/\epsilon^2\omega_0$.

3. Dimensionless governing equations

From here on we shall distinguish the physical variables by primes and consider a sea of constant depth h'. All gates have the thickness $2a'$ and width b', and are hinged along a straight axis on the bottom at $x' = 0, z' = -h'$. For simplicity we consider the simplest mode shown in figure 1, so that the modal period along the y'-axis is $2b'$. No long-scale spatial modulation in the y'-direction is considered. Other modal shapes discussed by Mei *et al.* (1994) can be treated similarly in principle.

If Θ' denotes the angular displacement of a gate, then to the leading order we have

$$\Theta'(y', t') = \left\{ \begin{array}{c} \Theta'^{I} \\ \Theta'^{II} \end{array} \right\} = \pm\theta'(t')\mathrm{e}^{-\mathrm{i}\omega_0 t'} + *, \quad \left\{ \begin{array}{l} 0 < y' < \frac{1}{2}b' \\ \frac{1}{2}b' < y' < b'. \end{array} \right. \tag{3.1}$$

Note that

$$\int_0^{b'} \Theta' \mathrm{d}y' = 0 \tag{3.2}$$

in order that no waves are radiated at the leading order. This mode is the most undesirable one from the engineering view point.

Let A'_T be the amplitude of the free-surface oscillation and ω_0 the natural frequency of the trapped modes. We introduce the following non-dimensional variables:

$$\boldsymbol{x} = (x, y, z) = \mathbf{x}'/b', \qquad t = \omega_0 t', \qquad \Phi = \Phi'/\omega_0 A'_T b', \qquad \zeta = \zeta'/A'_T, \tag{3.3}$$

where Φ' is the fluid velocity potential and ζ' is the free-surface elevation above $z' = 0$.

The non-dimensional water depth and gate half-thickness are

$$h = h'/b', \qquad a = a'/b'. \tag{3.4}$$

The dimensionless modal semi-period is now unity, $b = 1$. Let $\Omega^+(\Omega^-)$ denote the fluid regions to the right(left) of the gates, and distinguish quantities in $\Omega^\pm$ by the

superscripts $\pm$. Laplace and Bernoulli equations become respectively

$$\nabla^2 \Phi^{\pm} = 0, \tag{3.5}$$

$$-\frac{p'^{\pm}}{\rho \omega_0^2 b'^2} = Gz + \epsilon \Phi_t^{\pm} + \tfrac{1}{2}\epsilon^2 |\nabla \Phi^{\pm}|^2, \tag{3.6}$$

where

$$G = \frac{g}{\omega_0^2 b'} = O(1). \tag{3.7}$$

Thus $G^{-1/2}$ represents the non-dimensional eigenfrequency. The parameter $\epsilon = A'_T/b'$ is assumed to be much smaller than unity. On the free surface the dynamic condition is

$$-G\zeta^{\pm} = \Phi_t^{\pm} + \tfrac{1}{2}\epsilon |\nabla \Phi^{\pm}|^2, \qquad z = \epsilon \zeta^{\pm}, \tag{3.8}$$

while the combined kinematic–dynamic boundary condition is

$$\Phi_{tt}^{\pm} + G\Phi_z^{\pm} + \epsilon |\nabla \Phi^{\pm}|_t^2 + \tfrac{1}{2}\epsilon^2 \nabla \Phi^{\pm} \cdot \nabla |\nabla \Phi^{\pm}|^2 = 0, \qquad z = \epsilon \zeta^{\pm}. \tag{3.9}$$

On the bottom of the channel we impose the kinematic condition

$$\Phi_z^{\pm} = 0, \qquad z = -h. \tag{3.10}$$

Lastly, periodicity in y requires that

$$\Phi_y^{\pm} = 0, \qquad y = 0 \quad \text{and} \quad y = 1. \tag{3.11}$$

For a given angular displacement Θ', the amplitude of the associated wave is of the order of magnitude $h'\Theta'$. Since the angular displacement of the flapping gates must be of order $A'_T/h' \sim A'_T/b' = \epsilon$ radians, we normalize the angular displacement by $\epsilon = A'_T/b'$:

$$\Theta = \Theta'/\epsilon. \tag{3.12}$$

On a gate surface

$$x = \xi^{\pm} \equiv -(z+h)\tan \epsilon\Theta \pm \frac{a}{\cos \epsilon\Theta}, \tag{3.13}$$

the kinematic boundary condition is

$$\Phi_x^{\pm} = \Theta_t \frac{-(z+h) \pm a \sin \epsilon\Theta}{\cos^2 \epsilon\Theta} - \Phi_z^{\pm} \tan \epsilon\Theta. \tag{3.14}$$

Upon expressing the fluid pressure through Bernoulli equation (3.6), we obtain the equation of motion of gate I or II, which amounts to the dynamic boundary condition for the fluid:

$$\begin{aligned} I\epsilon\Theta_{tt} = {} & gS \sin \epsilon\Theta \\ & + \int_{y_1}^{y_2} \mathrm{d}y \left\{ - \int_{-h}^{\epsilon\zeta^+} \mathrm{d}z \left(Gz + \epsilon \Phi_t^+ + \tfrac{1}{2}\epsilon^2 |\nabla \Phi^+|^2 \right) \frac{(z + h - a \sin \epsilon\Theta)}{\cos^2 \epsilon\Theta} \right. \\ & \left. + \int_{-h}^{\epsilon\zeta^-} \mathrm{d}z \left(Gz + \epsilon \Phi_t^- + \tfrac{1}{2}\epsilon^2 |\nabla \Phi^-|^2 \right) \frac{(z + h + a \sin \epsilon\Theta)}{\cos^2 \epsilon\Theta} \right\}. \end{aligned} \tag{3.15}$$

In the above expression S and I are respectively the non-dimensional first and second moment of the gate about the bottom axis:

$$S = S'/\rho b'^4, \qquad I = I'/\rho b'^5, \tag{3.16}$$

and the non-dimensional limits of integration in y are $y_1 = 0$, $y_2 = 1/2$ for gate I and $y_1 = 1/2, y_2 = 1$ for gate II.

The gate boundary conditions (3.14) and (3.15) are nonlinear, as are those on the free surface.

4. Taylor expansion of boundary conditions

The free-surface boundary conditions (3.8) and (3.9), being given at $z = \epsilon\zeta$, can be Taylor-expanded about $z = 0$ in the usual manner. From the dynamic boundary condition (3.8) we obtain

$$-G\zeta^{\pm} = \left[\Phi_t^{\pm}\right]_{z=0} + \left[\Phi_{tz}^{\pm}\right]_{z=0}\epsilon\zeta + \tfrac{1}{2}\left[\Phi_{tzz}^{\pm}\right]_{z=0}\epsilon^2\zeta^2 + \left[\epsilon\tfrac{1}{2}|\nabla\Phi^{\pm}|^2\right]_{z=0} + \left[\epsilon\tfrac{1}{2}|\nabla\Phi^{\pm}|_z^2\right]_{z=0}\epsilon\zeta + O(\epsilon^3). \tag{4.1}$$

A similar expansion for the combined kinematic–dynamic boundary condition (3.9) yields

$$\left[\Phi_{tt}^{\pm} + G\Phi_z^{\pm}\right]_{z=0} + \left[\Phi_{ttz}^{\pm} + G\Phi_{zz}^{\pm}\right]_{z=0}\epsilon\zeta + \tfrac{1}{2}\left[\Phi_{ttzz}^{\pm} + G\Phi_{zzz}^{\pm}\right]_{z=0}\epsilon^2\zeta^2 + \left[\epsilon|\nabla\Phi^{\pm}|_t^2\right]_{z=0} + \left[\epsilon|\nabla\Phi^{\pm}|_t^2\right]_{z=0}\epsilon\zeta + \left[\epsilon^2\tfrac{1}{2}\nabla\Phi^{\pm}\cdot\nabla|\nabla\Phi^{\pm}|^2\right]_{z=0} + O(\epsilon^3) = 0. \tag{4.2}$$

We now treat the gate conditions. For small ϵ all the trigonometric functions in (3.13), (3.14) and (3.15) can be Taylor expanded about $\Theta = 0$; hence with an error of $O(\epsilon^3)$ the equation of the gate boundaries (3.13) is

$$x = \pm a - (z+h)\epsilon\Theta \pm \tfrac{1}{2}a\epsilon^2\Theta^2 + O(\epsilon^3). \tag{4.3}$$

To the same order of approximation, the kinematic boundary condition (3.14) on the gates is

$$\Phi_x^{\pm} = -(z+h)\Theta_t \pm a\epsilon\Theta\Theta_t - \Phi_z^{\pm}\epsilon\Theta - (z+h)\Theta_t\epsilon^2\Theta^2 + O(\epsilon^3). \tag{4.4}$$

In view of (4.3), the kinematic boundary condition on the gate can be expanded about the two vertical planes $x = \pm a$:

$$\begin{aligned}\left[\Phi_x^{\pm}\right]_{x=\pm a} = &-(z+h)\Theta_t + \epsilon\left\{(z+h)\Theta\left[\Phi_{xx}^{\pm}\right]_{x=\pm a} \pm a\Theta\Theta_t - \Theta\left[\Phi_z^{\pm}\right]_{x=\pm a}\right\} \\ &+ \epsilon^2\left\{\mp a\tfrac{1}{2}\Theta^2\left[\Phi_{xx}^{\pm}\right]_{x=\pm a} - \tfrac{1}{2}(z+h)^2\Theta^2\left[\Phi_{xxx}^{\pm}\right]_{x=\pm a} - (z+h)\Theta^2\Theta_t \right. \\ &\left. + (z+h)\Theta^2\left[\Phi_{zx}^{\pm}\right]_{x=\pm a}\right\} + O(\epsilon^3).\end{aligned} \tag{4.5}$$

Similar treatment of the equation of motion of the gate (3.15) gives

$$\begin{aligned}&I\Theta_{tt} + G\left[\tfrac{1}{2}ah^2 - S\right]\Theta + \epsilon^2\tfrac{1}{6}G\left[\tfrac{5}{2}ah^2 + S\right]\Theta^3 \\ &= \int_{y_1}^{y_2}\mathrm{d}y\int_{-h}^{0}\mathrm{d}z\left\{-\Delta\Phi_t(z+h)\right\} \\ &+ \epsilon\int_{y_1}^{y_2}\mathrm{d}y\int_{-h}^{0}\mathrm{d}z\left\{\Theta\Delta\Phi_{tx}(z+h)^2 + 2\Theta a\overline{\Phi_t} - \tfrac{1}{2}\Delta|\nabla\Phi|^2(z+h)\right\} \\ &- \epsilon^2\int_{y_1}^{y_2}\mathrm{d}y\int_{-h}^{0}\mathrm{d}z\left\{3\Theta^2 a\overline{\Phi_{tx}}(z+h) + \Theta^2\Delta\Phi_t(z+h) + \tfrac{1}{2}\Theta^2\Delta\Phi_{txx}(z+h)^3\right. \\ &\left. - \tfrac{1}{2}\Theta\Delta|\nabla\Phi|_x^2(z+h)^2 - a\Theta\overline{|\nabla\Phi|^2}\right\} - \epsilon\int_{y_1}^{y_2}\mathrm{d}y\left\{G\tfrac{1}{2}h\Delta\zeta^2 + h\Delta_0(\Phi_t\zeta)\right\}\end{aligned}$$

$$-\epsilon^2 \int_{y_1}^{y_2} \mathrm{d}y \left\{ G\left(\tfrac{1}{3}\Delta\zeta^3 - a\Theta\overline{\zeta^2} - h^2\Theta\Delta\zeta\zeta_x\right) + \tfrac{1}{2}h\Delta_0\left(\Phi_{tz}\zeta^2\right) + \tfrac{1}{2}\Delta_0\left(\Phi_t\zeta^2\right) \right.$$
$$\left. - \Theta h^2\Delta_0\left(\Phi_t\zeta\right)_x - 2\Theta a\overline{(\Phi_t\zeta)_0} + \tfrac{1}{2}h\Delta_0\left(|\nabla\Phi|^2\zeta\right)\right\} + O(\epsilon^3), \tag{4.6}$$

where Δf and $\overline{f}$ denote respectively the jump and the average of f on two sides of the gate:

$$\Delta(\cdot) = \left[(\cdot)^+\right]_{x=a} - \left[(\cdot)^-\right]_{x=-a}, \tag{4.7}$$

$$\overline{(\cdot)} = \tfrac{1}{2}\left\{\left[(\cdot)^+\right]_{x=a} + \left[(\cdot)^-\right]_{x=-a}\right\}. \tag{4.8}$$

Also, the jumps and averages at the waterline are denoted by

$$\Delta_0(\cdot) = \left[(\cdot)^+\right]_{x=a,z=0} - \left[(\cdot)^-\right]_{x=-a,z=0}, \tag{4.9}$$

$$\overline{(\cdot)_0} = \tfrac{1}{2}\left\{\left[(\cdot)^+\right]_{x=a,z=0} + \left[(\cdot)^-\right]_{x=-a,z=0}\right\}. \tag{4.10}$$

On the left-hand side of (4.6) the first, second and third terms are respectively the inertia term and the linear $O(1)$ and the nonlinear $O(\epsilon^2)$ buoyancy terms. On the right-hand side the first double integral is the linear $O(1)$ pressure torque. Indeed for $\epsilon = 0$ we recover the linear theory for a floating body. The nonlinear pressure torque at both $O(\epsilon)$ and $O(\epsilon^2)$ is composed of a surface integral in y and z and a line integral at $z = 0$. We stress that all the integrals in (4.6) are evaluated on the fixed planes $x = \pm a$.

5. Multiple-scale and harmonic expansions

In accordance with the estimates in §2, we introduce the slow time $t_2 = \epsilon^2 t$. The perturbation expansions of non-dimensional fluid velocity potential, free-surface elevation and gate rotation assume the forms

$$\left.\begin{aligned} \Phi^\pm &= \Phi_1^\pm(x,y,z,t,t_2) + \epsilon\Phi_2^\pm(x,y,z,t,t_2) + \epsilon^2\Phi_3^\pm(x,y,z,t,t_2) + \ldots, \\ \zeta^\pm &= \zeta_1^\pm(x,y,t,t_2) + \epsilon\zeta_2^\pm(x,y,t,t_2) + \epsilon^2\zeta_3^\pm(x,y,t,t_2) + \ldots, \\ \Theta &= \Theta_1(y,t,t_2) + \epsilon\Theta_2(y,\quad t,t_2) + \epsilon^2\Theta_3(y,t,t_2) + \ldots. \end{aligned}\right\} \tag{5.1}$$

The perturbation equations then follow from

the Laplace equation in $\Omega^\pm$ (3.5):

$$\nabla^2\Phi_n^\pm = 0, \qquad n = 1,2,3; \tag{5.2}$$

the free-surface boundary condition (4.2):

$$\Phi_{n_{tt}}^\pm + G\Phi_{n_z}^\pm = \mathscr{F}_n^\pm, \qquad z = 0, \tag{5.3}$$

where

$$\mathscr{F}_1^\pm = 0, \tag{5.4a}$$

$$\mathscr{F}_2^\pm = -\left[\left(\Phi_{1_{ttz}}^\pm + G\Phi_{1_{zz}}^\pm\right)\zeta_1^\pm + \left(\nabla\Phi_1^\pm\cdot\nabla\Phi_1^\pm\right)_t\right], \tag{5.4b}$$

$$\mathscr{F}_3^\pm = -\left[2\Phi_{1_{tt_2}}^\pm + \left(\Phi_{2_{tt}}^\pm + G\Phi_{2_z}^\pm\right)_z\zeta_1^\pm + \left(\Phi_{1_{tt}}^\pm + G\Phi_{1_z}^\pm\right)_z\zeta_2^\pm \right.$$
$$\left. + \tfrac{1}{2}\left(\Phi_{1_{tt}}^\pm + G\Phi_{1_z}^\pm\right)_{zz}\zeta_1^{\pm^2} + 2\left(\nabla\Phi_1^\pm\cdot\nabla\Phi_2^\pm\right)_t + \left(\nabla\Phi_1^\pm\cdot\nabla\Phi_1^\pm\right)_{tz}\zeta_1^\pm + \tfrac{1}{2}\nabla\Phi_1^\pm\cdot\nabla|\nabla\Phi_1^\pm|^2\right]; \tag{5.4c}$$

the free-surface dynamic boundary condition (4.1):

$$-G\zeta_n^{\pm} = \mathscr{B}_n^{\pm}, \qquad z = 0, \tag{5.5}$$

where

$$\mathscr{B}_1^{\pm} = \Phi_{1_t}^{\pm}, \tag{5.6a}$$

$$\mathscr{B}_2^{\pm} = \Phi_{2_t}^{\pm} + \zeta_1^{\pm}\Phi_{1_{tz}}^{\pm} + \tfrac{1}{2}|\nabla\Phi_1^{\pm}|^2, \tag{5.6b}$$

$$\mathscr{B}_3^{\pm} = \Phi_{3_t}^{\pm} + \zeta_1^{\pm}\Phi_{2_{tz}}^{\pm} + \zeta_2^{\pm}\Phi_{1_{tz}}^{\pm} + \nabla\Phi_1^{\pm}\cdot\nabla\Phi_2^{\pm} + \tfrac{1}{2}\zeta_1^{\pm^2}\Phi_{1_{tzz}}^{\pm} + \tfrac{1}{2}\zeta_1^{\pm}|\nabla\Phi_1^{\pm}|_z^2 + \Phi_{1_{t_2}}^{\pm}. \tag{5.6c}$$

the bottom boundary condition (3.10):

$$\Phi_{n_z}^{\pm} = 0, \qquad z = -h; \tag{5.7}$$

the periodicity condition (3.11):

$$\Phi_{n_y}^{\pm} = 0, \qquad y = 0, \quad y = 1; \tag{5.8}$$

the kinematic boundary condition on one gate (4.5):

$$\Phi_{n_x}^{\pm} = -(z+h)\Theta_{n_t} + \mathscr{G}_n^{\pm}, \qquad x = \pm a, \tag{5.9}$$

where

$$\mathscr{G}_1^{\pm} = 0, \tag{5.10a}$$

$$\mathscr{G}_2^{\pm} = (z+h)\Theta_1\Phi_{1_{xx}}^{\pm} \pm a\Theta_1\Theta_{1_t} - \Theta_1\Phi_{1_z}^{\pm}, \tag{5.10b}$$

$$\begin{aligned}\mathscr{G}_3^{\pm} = {} & (z+h)\left(\Theta_1\Phi_{2_{xx}}^{\pm} + \Theta_2\Phi_{1_{xx}}^{\pm} - \Theta_1^2\Theta_{1_t} + \Theta_1^2\Phi_{1_{zx}}^{\pm} - \Theta_{1_{t_2}}\right) \\ & -(z+h)^2\tfrac{1}{2}\Theta_1^2\Phi_{1_{xxx}}^{\pm} \pm a\left(\Theta_1\Theta_2\right)_t - \Theta_1\Phi_{2_z}^{\pm} - \Theta_2\Phi_{1_z}^{\pm} \mp a\tfrac{1}{2}\Theta^2\Phi_{1_{xx}}^{\pm};\end{aligned} \tag{5.10c}$$

the equation of gate motion (4.6):

$$I\Theta_{n_{tt}} + GC\Theta_n = \int_{y_1}^{y_2}\mathrm{d}y\int_{-h}^{0}\mathrm{d}z\,\{-\Delta\Phi_{n_t}(z+h)\} + \mathscr{D}_n, \tag{5.11}$$

where

$$\mathscr{D}_1 = 0, \tag{5.12a}$$

$$\begin{aligned}\mathscr{D}_2 = {} & \int_{y_1}^{y_2}\mathrm{d}y\int_{-h}^{0}\mathrm{d}z\left\{-\tfrac{1}{2}\Delta|\nabla\Phi_1|^2(z+h) + \Theta_1\Delta\Phi_{1_{tx}}(z+h)^2 + 2\Theta_1\overline{a\Phi_{1_t}}\right\} \\ & -\int_{y_1}^{y_2}\mathrm{d}y\left\{G\tfrac{1}{2}h\Delta\zeta_1^2 - h\Delta_0\left(\Phi_{1_t}\zeta_1\right)\right\},\end{aligned} \tag{5.12b}$$

$$\begin{aligned}\mathscr{D}_3 = {} & \int_{y_1}^{y_2}\mathrm{d}y\int_{-h}^{0}\mathrm{d}z\Big\{-\left[\Delta\left(\nabla\Phi_1\cdot\nabla\Phi_2\right) + 3\Theta_1^2\overline{a\Phi_{1_{tx}}} + \Theta_1^2\Delta\Phi_{1_t} + \Delta\Phi_{1_{t_2}}\right](z+h) \\ & + \left(\Theta_1\Delta\Phi_{2_{tx}} + \Theta_2\Delta\Phi_{1_{tx}} + \tfrac{1}{2}\Theta_1\Delta|\nabla\Phi_1|_x^2\right)(z+h)^2 + \\ & -\tfrac{1}{2}\Theta_1^2\Delta\Phi_{1_{txx}}(z+h)^3 + 2\Theta_1\overline{a\Phi_{2_t}} + 2\Theta_2\overline{a\Phi_{1_t}} + a\Theta_1\overline{|\nabla\Phi_1|^2}\Big\} \\ & -\int_{y_1}^{y_2}\mathrm{d}y\Big\{h\Delta_0\left(\Phi_{1_t}\zeta_2\right) - h\Delta_0\left(\Phi_{2_t}\zeta_1\right) - \tfrac{1}{2}h\Delta_0\left(\Phi_{1_{tz}}\zeta_1^2\right) - \tfrac{1}{2}\Delta_0\left(\Phi_{1_t}\zeta_1^2\right) \\ & -G\left[h\Delta\left(\zeta_1\zeta_2\right) + \tfrac{1}{3}\Delta\zeta_1^3 - a\Theta_1\overline{\zeta_1^2} - h^2\Theta_1\Delta\zeta_1\zeta_{1_x}\right] \\ & +\Theta_1h^2\Delta_0\left(\Phi_{1_t}\zeta_1\right)_x + 2\Theta_1\overline{a\left(\Phi_{1_t}\zeta_1\right)_0} - \tfrac{1}{2}h\Delta_0\left(|\nabla\Phi_1|^2\zeta_1\right)\Big\} \\ & -\tfrac{1}{6}G\left[\tfrac{5}{2}ah^2 + S\right]\Theta_1^3 - 2I\Theta_{1_{tt_2}},\end{aligned} \tag{5.12c}$$

and

$$C = \tfrac{1}{2}ah^2 - S \tag{5.13}$$

is the non-dimensional buoyancy of the gate.

As seen in the Introduction, the incident wave amplitude A' must be an order smaller than the trapped wave, i.e. $A'/A'_T = O(\epsilon)$. Accordingly we shall introduce a normalized amplitude $A_2 = O(1)$ of the incident wave by

$$A' = \epsilon^2 b' A_2 = \epsilon A'_T A_2. \tag{5.14}$$

Let there be a small detuning so that the dimensionless incident wave frequency is $2\left(1 + \Delta\omega/\omega_0\right)$. In order for its contribution to be comparable to the cubic terms and the slow growth, we let $\Delta\omega/\omega_0 = \epsilon^2\omega_2$ where $\omega_2 = O(1)$.

Let us now assume the following harmonic expansions at each order n:

$$\left\{\Phi_n^{\pm}, \zeta_n^{\pm}, \Theta_n\right\} = \sum_{m=-n}^{n} \left\{\phi_{nm}^{\pm}, \eta_{nm}^{\pm}, \theta_{nm}\right\} \mathrm{e}^{-\mathrm{i}m(1+\epsilon^2\omega_2)t}. \tag{5.15}$$

For the functions $\left\{\phi_{nm}^{\pm}, \eta_{nm}^{\pm}, \theta_{nm}\right\}$ to be real we also require

$$\left\{\phi_{nm}^{\pm}, \eta_{nm}^{\pm}, \theta_{nm}\right\} = \left\{\phi_{n,-m}^{\pm}, \eta_{n,-m}^{\pm}, \theta_{n,-m}\right\}^*, \tag{5.16}$$

and $\left\{\phi_{n0}^{\pm}, \eta_{n0}^{\pm}, \theta_{n0}\right\}$ to be real, where the superscripts * signify the complex conjugate of the given quantity. Also the forcing terms in (5.3), (5.5), (5.9) and (5.11) can be expanded similarly:

$$\left\{\mathscr{F}_n^{\pm}, \mathscr{B}_n^{\pm}, \mathscr{G}_n^{\pm}, \mathscr{D}_n\right\} = \sum_{m=-n}^{n} \left\{\mathscr{F}_{nm}^{\pm}, \mathscr{B}_{nm}^{\pm}, \mathscr{G}_{nm}^{\pm}, \mathscr{D}_{nm}\right\} \mathrm{e}^{-\mathrm{i}m(1+\epsilon^2\omega_2)t}, \tag{5.17}$$

with

$$\left\{\mathscr{F}_{nm}^{\pm}, \mathscr{B}_{nm}^{\pm}, \mathscr{G}_{nm}^{\pm}, \mathscr{D}_{nm}\right\} = \left\{\mathscr{F}_{n,-m}^{\pm}, \mathscr{B}_{n,-m}^{\pm}, \mathscr{G}_{n,-m}^{\pm}, \mathscr{D}_{n,-m}\right\}^* \tag{5.18}$$

and $\left\{\mathscr{F}_{n0}^{\pm}, \mathscr{B}_{n0}^{\pm}, \mathscr{G}_{n0}^{\pm}, \mathscr{D}_{n0}\right\}$ being real. To simplify the notation we shall redefine the longitudinal coordinate so that x replaces $x \mp a$ in $\Omega^{\pm}$.

Upon substitution of the harmonic expansions (5.15) into the governing equations, we get a sequence of boundary value problems in (x, y, z) at each order n and harmonic component m:

$$\nabla^2\phi_{nm}^{\pm} = 0, \qquad \text{in} \quad \Omega^{\pm}, \tag{5.19}$$

$$G\phi_{nm_z}^{\pm} - m^2\phi_{nm} = \mathscr{F}_{nm}^{\pm}, \qquad z = 0, \tag{5.20}$$

$$\phi_{nm_z}^{\pm} = 0, \qquad z = -h, \tag{5.21}$$

$$\phi_{nm_y}^{\pm} = 0, \qquad y = 0,\ y = 1 \tag{5.22}$$

$$\phi_{nm_x}^{\pm} - \mathrm{i}m(z+h)\theta_{nm} = \mathscr{G}_{nm}^{\pm}, \qquad x = 0, \tag{5.23}$$

which must be solved jointly with the equation of the gate motion for θ_{nm}

$$-m^2 I\theta_{nm} + GC\theta_{nm} = \mathrm{i}m\int_{y_1}^{y_2} \mathrm{d}y \int_{-h}^{0} \mathrm{d}z(z+h)\Delta\phi_{nm} + \mathscr{D}_{nm}, \qquad x = 0, \tag{5.24}$$

and the condition of periodicity in y,

$$\phi_{nm_y}^{\pm} = 0, \qquad y = 0 \quad \text{and} \quad y = 1. \tag{5.25}$$

The boundary value problems for the first and second orders must be solved sequentially. The condition of solvability for the first harmonic at the third order then gives the evolution equation.

6. First-order problem: the trapped mode

At $O(1)$, the boundary value problem for the zeroth harmonic $\phi_{10}^{\pm}$ is homogeneous, since all forcing terms are zero: $\mathscr{F}_{10}^{\pm} = \mathscr{B}_{10}^{\pm} = \mathscr{G}_{10}^{\pm} = \mathscr{D}_{10} = 0$. The solution is therefore simply $\phi_{10}^{\pm} = \phi_{10}^{\pm}(t_2)$. The corresponding angular drift θ_{10} vanishes.

The first-harmonic potential corresponds to the trapped wave, and has been solved by Mei *et al.* (1994). For later use we cite the key results here and comment on the physical implications.

All the forcing terms in the governing equations are zero: $\mathscr{F}_{11}^{\pm} = \mathscr{B}_{11}^{\pm} = \mathscr{G}_{11}^{\pm} = \mathscr{D}_{11} = 0$. The kinematic condition on the gate surface (5.9) gives

$$\phi_{11_x}^{\pm} = \mathrm{i}(z+h)\theta_{11}, \qquad x = 0. \tag{6.1}$$

The motion of the gate is governed by

$$-I\theta_{11} + GC\theta_{11} = \mathrm{i}\int_{y_1}^{y_2} \mathrm{d}y \int_{-h}^{0} \mathrm{d}z(z+h)\Delta\phi_{11}, \tag{6.2}$$

which is the dynamic boundary condition on the gate surface.

In accordance with (3.1), we express $\theta_{11}(t_2)$ as

$$\theta_{11} = \theta q_{11} \tag{6.3}$$

where q_{11} is the modal shape

$$q_{11} = \begin{cases} 1, & 0 < y < \frac{1}{2} \\ -1, & \frac{1}{2} < y < 1 \end{cases} \tag{6.4}$$

which can be expanded in cosine series

$$q_{11} = \sum_{m=1}^{\infty} \left(\frac{4}{m\pi} \sin\frac{m\pi}{2} \right) \cos m\pi y. \tag{6.5}$$

Note that (3.2) is satisfied. The corresponding potential satisfying (6.1) is readily found to be

$$\phi_{11}^{\pm} = \mp\mathrm{i}\theta \sum_{m=1}^{\infty}\sum_{n=0}^{\infty} \beta_{mn} \cos m\pi y \ \cosh K_n(z+h)\, \mathrm{e}^{\mp\alpha_{mn}x} \equiv \mp\mathrm{i}\theta f_{11}^{\pm}(x,y,z). \tag{6.6}$$

while free-surface displacement is

$$\eta_{11}^{\pm} = \pm\frac{\theta}{G} \sum_{m=1}^{\infty}\sum_{n=0}^{\infty} \beta_{mn} \cos m\pi y \ \cosh K_n h\, \mathrm{e}^{\mp\alpha_{mn}x} = \pm\frac{\theta}{G} f_{11}^{\pm}(x,y,0) \tag{6.7}$$

with K_n defined by

$$K_n = \begin{cases} k & \text{for } n = 0 \\ \mathrm{i}k_n & \text{for } n = 1,2,\ldots \end{cases} \tag{6.8}$$

with k and k_n being the real roots of

$$1 = Gk\tanh kh \quad \text{and} \quad 1 = -Gk_n \tan k_n h, \quad n = 1,2,\ldots, \tag{6.9}$$

respectively. For all $m = 1, 2, \ldots$ and n, the real coefficients α_{mn}, β_{mn} are defined by

$$\alpha_{mn} = \left(m^2\pi^2 - K_n^2\right)^{1/2}, \tag{6.10}$$

$$\beta_{mn} = \frac{8 \sin \frac{1}{2}m\pi \left[\left(h/G - 1\right) \cosh K_n h + 1\right]}{m\pi\alpha_{mn} K_n^2 \left(h + G \sinh^2 K_n h\right)}. \tag{6.11}$$

Since $\beta_{00} = 0$, no plane waves are radiated to infinity.

To disallow the radiation of cross-waves, it is necessary that $k < \pi$, which guarantees that the α_{mn} are all real. Hence all modes in (6.6) are evanescent, and $\phi_{11}^{\pm}$ is a trapped wave. Note that the real function $f_{11}^{\pm}(x, y, z)$ defined by (6.6) has the following symmetry properties about the $x = 0$ plane:

$$f_{11}^{+}(x, y, z) = f_{11}^{-}(-x, y, z), \quad f_{11_x}^{+}(x, y, z) = -f_{11_x}^{-}(-x, y, z). \tag{6.12}$$

Using the potential (6.6) to calculate the pressure torque, and applying the dynamic boundary condition (6.2) on each gate, we obtain one and the same eigenvalue condition for $G = g/\omega_0^2 b'$:

$$-I + GC = I_a(G), \tag{6.13}$$

where $I_a(G)$ is the added hydrodynamic inertia defined as

$$I_a(G) = \frac{2}{\pi} \sum_{m=1}^{\infty} \sum_{n=0}^{\infty} \frac{\beta_{mn} D_n}{m} \sin \frac{m\pi}{2} \tag{6.14}$$

and

$$D_n = \int_{-h}^{0} \mathrm{d}z \, (z + h) \cosh K_n (z + h) = \frac{1}{K_n^2} \left[\left(\frac{h}{G} - 1\right) \cosh K_n h + 1\right]. \tag{6.15}$$

The solution of (6.13) has been confirmed experimentally (Mei *et al.* 1994) for a model gate in the laboratory. To better understand the practical implications we briefly examine the parametric dependence of G, which is proportional to the square of the eigenperiod, on the geometry and inertia of the gates a, S, I and the depth of the channel h. For simplicity we replace the hollow gate by a light and homogeneous block of constant density ρ_g, with height $h_g' > h'$, width $b'/2$, thickness $2a'$. It can be shown that

$$S' = \rho_g a' \tfrac{1}{2} b' h_g'^2, \qquad I' = \tfrac{2}{3} \rho_g a' \tfrac{1}{2} b' h_g'^3, \tag{6.16}$$

so that

$$S' = \alpha I' \quad \text{and} \quad \alpha = \frac{3}{2h_g'}. \tag{6.17}$$

Therefore, for a fixed displaced volume $a'b'h'$, the first and second moments S' and I' can be varied together by varying ρ_g.

Returning to non-dimensional variables, let us first vary the gate moments, S and I (by varying gate density ρ_g), and gate thickness a, for fixed water depth $h = 1$. In figure 2 we set $\alpha = 0.65$. Clearly G increases for decreasing a or increasing I. Thus the eigenperiods can be increased by decreasing the displacement volume or increasing the inertia of the gate. Note that in the limit of a weightless gate $(S, I) \to 0$, G approaches the finite limit

$$G_0 = \frac{I_a(G_0)}{\frac{1}{2}ah^2}, \tag{6.18}$$

as can be inferred from (6.13). In this limit, inertia is contributed only by the

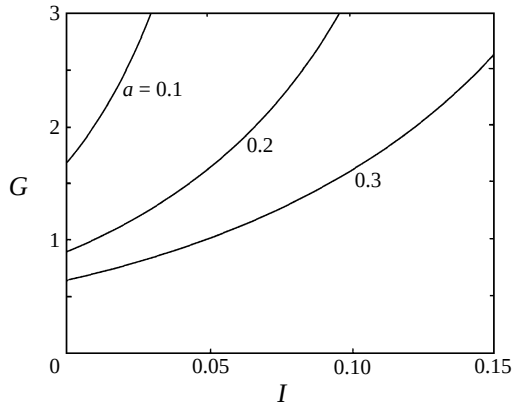

FIGURE 2. Normalized eigenperiod G for fixed $h = 1$ and varying $S = 0.65I$; $a = 0.1$, 0.2 and 0.3.

displaced fluid. For a fixed gate thickness a, G becomes unbounded as $S = \alpha I$ is increased toward the value $S = ah^2/2$ which renders $C = 0$. Thus resonance by an incident wave of known period can be avoided by increasing the gate inertia, i.e. increasing the eigenperiod. On the other hand, for fixed S or I, an increase in a, meaning increasing displacement, shortens the natural period.

Similar dependence is observed when we fix the thickness a and test the dependence on S (and I) and the water depth h (Sammarco 1996). For a fixed h, increasing I leads to increasing G and for a fixed I, increasing h shortens the natural period.

For each water depth h, the necessary condition for the existence of the trapped wave is the absence of short-crested propagating waves, $k < \pi$, or, in view of (6.9)

$$G > \frac{1}{\pi \tanh \pi h}. \tag{6.19}$$

This implies a cutoff frequency

$$\left(\frac{g}{b'}\pi \tanh \pi \frac{h'}{b'}\right)^{1/2}, \tag{6.20}$$

which increases with increasing h' or decreasing b'. Since G decreases as a and h increase, there is always a threshold for a and h beyond which (6.19) is not satisfied and trapped modes are not possible. Thus if buoyancy and restoring force are too large (large a or h), waves are radiated at the first order and no trapped wave is possible. Between the above two limits, G is a monotonic continuous function of a and h.

We do not discuss other modes in which more gates are involved in a spatial period. It can be shown (Mei *et al.* 1994) that these modes correspond to longer natural periods and smaller phase difference between adjacent gates, hence pose less danger to the design.

7. Second-order problems: diffraction and radiation

7.1. *Zeroth harmonic*

At the second order, the zeroth harmonic is forced by the trapped wave through quadratic nonlinearities. In view of (6.3), (6.6) and (6.7), $|\theta|^2$ can be factored from the forcing terms of the zeroth harmonic in (5.20)–(5.24), leaving only the real coefficients

$f_{11}^{\pm}$ and q_{11}. The forcing terms are of the form $\phi_{11}\eta_{11}^{*} + \phi_{11}^{*}\eta_{11}$ in the mixed condition on the free surface or $\phi_{11}\theta_{11}^{*} + \phi_{11}^{*}\theta_{11}$ in the kinematic condition on the gate surface. Since ϕ_{11} is proportional to $\mathrm{i}\theta$ and consists of evanescent modes only, and since η_{11} and θ_{11} are proportional to θ, it follows that

$$\phi_{11}\eta_{11}^{*} + \phi_{11}^{*}\eta_{11} = -\frac{\mathrm{i}}{G}\theta\theta^{*}f_{11}f_{11} + \frac{\mathrm{i}}{G}\theta^{*}\theta f_{11}f_{11} \equiv 0, \tag{7.1}$$

and

$$\phi_{11}\theta_{11}^{*} + \phi_{11}^{*}\theta_{11} = -\mathrm{i}\theta\theta^{*}f_{11}q_{11} + \mathrm{i}\theta^{*}\theta f_{11}q_{11} \equiv 0. \tag{7.2}$$

By similar reasoning the forcing terms are all zero:

$$\mathscr{F}_{20}^{\pm} = \mathscr{G}_{20}^{\pm} = \mathscr{D}_{20} = 0. \tag{7.3}$$

In deducing the last result for $\mathscr{D}_{20}$ use has been made of the symmetry properties (6.12), which ensures the vanishing of all the jumps $\Delta(\cdot)$ and averages $\overline{(\cdot)}$ across the gate.

Now the boundary value problem coupling $\phi_{20}^{\pm}$ and θ_{20} is identical to that governing ϕ_{10}, so that

$$\phi_{20} = \phi_{20}(t_2) \quad \text{and} \quad \theta_{20} = 0, \tag{7.4}$$

i.e. the trapped wave does not induce any drift in the angular displacement. However

$$\mathscr{B}_{20}^{\pm} = -\mathrm{i}\phi_{11_z}^{\pm}\eta_{11}^{\pm^{*}} + \mathrm{i}\phi_{11_z}^{\pm^{*}}\eta_{11}^{\pm} + \nabla\phi_{11}^{\pm}\cdot\nabla\phi_{11}^{\pm^{*}} = |\theta|^2\left(\frac{2}{G}f_{11_z}^{\pm}f_{11}^{\pm} + |\nabla f_{11}^{\pm}|^2\right), \tag{7.5}$$

hence a set-down $\eta_{20}^{\pm}(x, y)$ is induced:

$$\eta_{20}^{\pm} = -\frac{1}{G}|\theta|^2\left(\frac{2}{G}f_{11_z}^{\pm}f_{11}^{\pm} + |\nabla f_{11}^{\pm}|^2\right), \tag{7.6}$$

which is symmetrical with respect to $x = 0$: $\eta_{20}^{+}(x, y) = \eta_{20}^{-}(-x, y)$, consistent with the fact that the mean angular displacement is zero.

7.2. *First harmonic*

The forcing terms of the first harmonic are given by the quadratic products of the spatial gradients of (ϕ_{10}, η_{10}) and (ϕ_{11}, η_{11}). These products are all zero because ϕ_{10} depends only on t_2 and $q_{10} = 0$. Hence, the forcing terms of the first harmonic ϕ_{21} are all zero, $\mathscr{F}_{21}^{\pm} = \mathscr{B}_{21}^{\pm} = \mathscr{G}_{21}^{\pm} = \mathscr{D}_{21} = 0$, and the boundary value problem governing ϕ_{21} is homogeneous and identical to that governing the trapped wave mode ϕ_{11}. Without loss of generality we set $\phi_{21}^{\pm} = \theta_{21} = \eta_{21}^{\pm} = 0$.

7.3. *Second harmonic*

From the form of the forcing terms we can split the second-harmonic potential into two parts as follows:

$$\phi_{22}^{\pm} = \phi_{22}^{(\theta)} + \phi_{22}^{(A)} \equiv \mathrm{i}\theta^2 f_{22}^{\pm}(x, y, z) + \mathrm{i}A_2 g_{22}^{\pm}(x, z), \tag{7.7}$$

where $f_{22}^{\pm}$ and $g_{22}^{\pm}$ are complex functions defined by inhomogeneous boundary value problems sketched in the Appendix. With the lengthy details of solution to be found in Sammarco (1996), it suffices to say that the first part $f_{22}^{\pm}$ is forced by quadratic nonlinearities associated with the trapped wave, and leads to radiation damping. The second part $g_{22}^{\pm}$ is forced by the incident wave $A' = b'\epsilon^2 A_2$, with $A_2 = O(1)$. After their solution the gate rotation θ_{22} and the free-surface displacement $\eta_{22}^{\pm}$ can be found.

8. Third-order problem: the evolution equation

At this order our goal is only to invoke the solvability of the inhomogeneous problem for the first harmonic, the homogeneous solution being the trapped wave potential ϕ_{11}. The forcing terms are lengthy and can be found in Sammarco (1996). Let us apply Green's formula to $\phi_{11}^{\pm}$ and $\phi_{31}^{\pm}$ in both domains $\Omega^{\pm}$ defined by the modal period $0 < y < 1$:

$$\iiint_{\Omega^{\pm}} \left(\phi_{11}^{\pm}\nabla^2\phi_{31}^{\pm} - \phi_{31}^{\pm}\nabla^2\phi_{11}^{\pm}\right) \mathrm{d}\Omega = \iint_{\partial\Omega^{\pm}} \left(\phi_{11}^{\pm}\frac{\partial\phi_{31}^{\pm}}{\partial n} - \phi_{31}^{\pm}\frac{\partial\phi_{11}^{\pm}}{\partial n}\right) \mathrm{d}S, \tag{8.1}$$

where $\partial\Omega^{\pm}$ consists of the gate surfaces at $x = \pm 0$, the free surface, the seabed and the vertical section at $x \sim \pm\infty$. Using the governing equations for $\phi_{11}^{\pm}$ and $\phi_{31}^{\pm}$ and the boundary condition on the free surface, the kinematic condition on the gate and the property $\phi_{11}^{\pm}, \phi_{11_x}^{\pm} \to 0$ as $x \to \pm\infty$, we get

$$\begin{aligned} 0 = \mp \int_0^1 \mathrm{d}y \int_{-h}^0 \mathrm{d}z \left\{\phi_{11}^{\pm}\left[\mathrm{i}(z+h)\theta_{31} + \mathscr{G}_{31}^{\pm}\right] - \phi_{31}^{\pm}\left[\mathrm{i}(z+h)\theta_{11}\right]\right\}_{x=\pm 0} \\ \pm \frac{1}{G}\int_0^{\pm\infty} \mathrm{d}x \int_0^1 \mathrm{d}y \phi_{11}^{\pm}\mathscr{F}_{31}^{\pm}, \end{aligned} \tag{8.2}$$

where $\mathscr{F}_{31}$ and $\mathscr{G}_{31}$ are the first harmonics of the forcing terms on the free surface (5.4c) and gate surface (5.10c) respectively.

The sum of this equation for two opposite sides, i.e. $(8.2)^+$ and $(8.2)^-$, gives

$$\begin{aligned} 0 = \frac{1}{G}\int_0^1 \mathrm{d}y \left\{\int_{-\infty}^0 \mathrm{d}x \phi_{11}^{-}\mathscr{F}_{31}^{-} + \int_0^{\infty} \mathrm{d}x \phi_{11}^{+}\mathscr{F}_{31}^{+}\right\} - \int_0^1 \mathrm{d}y \int_{-h}^0 \mathrm{d}z \Delta\left(\phi_{11}\mathscr{G}_{31}\right) \\ -\mathrm{i}\int_0^1 \mathrm{d}y \int_{-h}^0 \mathrm{d}z \left[\Delta\phi_{11}\theta_{31} - \Delta\phi_{31}\theta_{11}\right](z+h). \end{aligned} \tag{8.3}$$

On the right-hand side of the last integral, θ_{31} and $\phi_{31}^{\pm}$ are still unknown. We now make use of the dynamical boundary condition on the gates. Let θ_{31} be expressed by

$$\theta_{31} = \begin{cases} \theta_{31}^{I} & \text{for} \quad 0 < y < \frac{1}{2} \\ \theta_{31}^{II} & \text{for} \quad \frac{1}{2} < y < 1. \end{cases} \tag{8.4}$$

Multiplying (6.2) by θ_{31} we get for gates I and II separately

$$(-I + GC)\,\theta_{11}^{I}\theta_{31}^{I} = \mathrm{i}\int_0^{1/2} \mathrm{d}y \int_{-h}^0 \mathrm{d}z \left\{\Delta\phi_{11}\theta_{31}^{I}(z+h)\right\}, \tag{8.5}$$

$$(-I + GC)\,\theta_{11}^{II}\theta_{31}^{II} = \mathrm{i}\int_{1/2}^1 \mathrm{d}y \int_{-h}^0 \mathrm{d}z \left\{\Delta\phi_{11}\theta_{31}^{II}(z+h)\right\}. \tag{8.6}$$

Similarly, multiplying (5.24) for θ_{31} by θ_{11} yields for gates I and II separately

$$(-I + GC)\,\theta_{31}^{I}\theta_{11}^{I} = \mathrm{i}\int_0^{1/2} \mathrm{d}y \int_{-h}^0 \mathrm{d}z \left\{\Delta\phi_{31}\theta_{11}^{I}(z+h)\right\} + \mathscr{D}_{31}^{I}\theta_{11}^{I}, \tag{8.7}$$

$$(-I + GC)\,\theta_{31}^{II}\theta_{11}^{II} = \mathrm{i}\int_{1/2}^1 \mathrm{d}y \int_{-h}^0 \mathrm{d}z \left\{\Delta\phi_{31}\theta_{11}^{II}(z+h)\right\} + \mathscr{D}_{31}^{II}\theta_{11}^{II}, \tag{8.8}$$

where $\mathscr{D}_{31}^{I}$ and $\mathscr{D}_{31}^{II}$ represent the first harmonic of (5.12c) for gate I ($y_1 = 0, y_2 = 1/2$) and gate II ($y_1 = 1/2, y_2 = 1$) respectively.

Subtracting the sum of (8.7) and (8.8) from the sum of (8.5) and (8.6) we get

$$0 = \mathrm{i}\int_0^1 \mathrm{d}y \int_{-h}^0 \mathrm{d}z\,[\Delta\phi_{11}\theta_{31} - \Delta\phi_{31}\theta_{11}]\,(z+h) - \mathscr{D}^I_{31}\theta^I_{11} - \mathscr{D}^{II}_{31}\theta^{II}_{11}. \tag{8.9}$$

The first integral on the right-hand side is just the last integral in Green's formula (8.3). Hence the latter can be expressed in terms of only the forcing terms $\mathscr{F}_{31}, \mathscr{G}_{31}, \mathscr{D}_{31}$,

$$0 = \frac{1}{G}\int_0^1 \mathrm{d}y \left\{\int_{-\infty}^0 \mathrm{d}x\phi^-_{11}\mathscr{F}^-_{31} + \int_0^\infty \mathrm{d}x\phi^+_{11}\mathscr{F}^+_{31}\right\} - \int_0^1 \mathrm{d}y \int_{-h}^0 \mathrm{d}z\Delta\,(\phi_{11}\mathscr{G}_{31}) - \sum \mathscr{D}_{31}\theta_{11}, \tag{8.10}$$

where

$$\sum \mathscr{D}_{31}\theta_{11} \equiv \mathscr{D}^I_{31}\theta^I_{11} + \mathscr{D}^{II}_{31}\theta^{II}_{11}. \tag{8.11}$$

Carrying out the integrals, the right-hand side of (8.10) gives finally the following evolution equation of Landau–Stuart form:

$$-\mathrm{i}C_T\theta_{t_2} = \omega_2 C_T\theta + \theta^2\theta^*\,(C_N + \mathrm{i}C_R) + A_2\theta^* C_F. \tag{8.12}$$

With details of the calculations given in Sammarco (1996), we simply state that the coefficient C_T is always non-zero. The coefficients C_N, C_R, C_F represent respectively nonlinearity, radiation damping and forcing by the incident wave. They are respectively composed of an integral on the free surface, on the gate surface and on the waterline $x = 0, z = 0$. The coefficient C_F can be evaluated analytically in a straightforward manner. The evaluation of C_N and C_R is more involved since it contains the products of f^+_{22} and f^+_{11}: numerical integration is used, which is computationally more expedient than the summation of the series resulting from analytical integrations. Dividing (8.12) by C_T we formally reduce the coefficients to three:

$$-\mathrm{i}\theta_{t_2} = \omega_2\theta + \theta^2\theta^*\,(c_N + \mathrm{i}c_R) + A_2\theta^* c_F. \tag{8.13}$$

In summary, we have found the evolution equation which describes the evolution of the amplitude of the trapped wave θ for a given incident wave amplitude A_2. All the coefficients C_T and $\{c_N, c_R, c_F\} = \{C_N, C_R, C_F\}/C_T$ depend on the non-dimensional thickness a and inertial characteristics S, I of the gate both explicitly (c_N and c_R) and implicitly through G. The dependence on the non-dimensional water depth h is present in all coefficients, both explicitly and implicitly, through G. Sample values of the coefficients are shown in figure 3(*a–d*).

In physical variables, the evolution equation for the complex amplitude of the gate motion in radians, θ', is

$$-\frac{\mathrm{i}}{\omega_0}\theta'_{t'} = \frac{\Delta\omega}{\omega_0}\theta' + \theta'^2\theta'^*\,(c_N + \mathrm{i}c_R) + \frac{A'}{b'}\theta'^* c_F. \tag{8.14}$$

9. Corrections for friction

Dissipation is inevitable in the boundary layers on the gate surface, at the bottom surface and at the vertical walls of a laboratory flume. The fluid shear stress also exerts a torque on the gate. All these effects contribute to the reduction of gate amplitude. In past theories on edge waves on a laboratory beach, or Faraday waves in a container, the effects of viscous boundary layers are modelled in an *ad hoc* manner by a linear term with a real damping coefficient, β, say. It is known for simple progressive or standing waves that the boundary layer effects result in a complex damping coefficient $\beta(1 + \mathrm{i})$ which affects both the amplitude and phase of oscillations. For the present

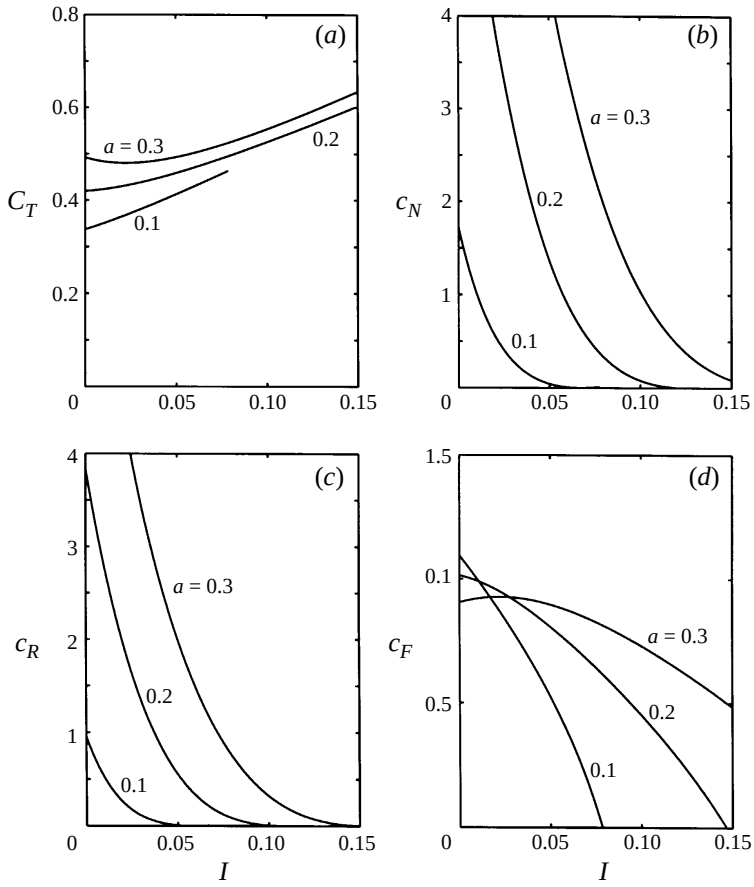

FIGURE 3. Coefficients of the evolution equations for fixed $h = 1$ and varying $S = 0.65I$; $a = 0.1$, 0.2 and 0.3

problem, the same can be shown by a formal perturbation analysis, in the manner of Johns (1968), Dore (1969), Greenspan (1968), Mei & Liu (1973), and Mei (1989) (see Sammarco 1996). The precise value of the viscous damping coefficient is however difficult to predict due to other factors such as surface contamination and the meniscus along the waterline. We shall therefore determine the numerical factor by experiments to be described shortly.

At higher amplitudes, flow separation occurs near sharp corners of the laboratory model as well the prototype. A hydraulic argument can be made to add a torque which accounts for the effects of vortex shedding (Mei 1989, p. 254 ff.). By this argument Sammarco (1996) has shown that a term proportional to $i|\theta|\theta$ can be added on the right of (8.12) with the coefficient of proportionality estimated crudely by

$$c_Q C_T \sim \frac{1}{24\pi}\left(\frac{h'}{b'}\right)^4\left(\frac{1}{c_c}-1\right)^2. \tag{9.1}$$

The contraction coefficient c_c is an empirical quantity which is slightly less than unity for not very sharp corners. Hence c_Q is small and justifies the appearance of the quadratic loss at $O(\epsilon^3)$. We shall resort to experiments to find an accurate value for c_Q.

In summary the final evolution equation in dimensional form is

$$-\frac{\mathrm{i}}{\omega_0}\theta'_{t'} = \frac{\Delta\omega}{\omega_0}\theta' + \theta'^2\theta'^*(c_N + \mathrm{i}c_R) + \frac{A'}{b'}\theta'^* c_F + (1+\mathrm{i})\,c_L\theta' + \mathrm{i}c_Q|\theta'|\theta'. \tag{9.2}$$

For application of (9.2) to gate motion forced by incident waves, it is necessary to determine the damping coefficients c_L and c_Q. Their values must depend on the scales of the laboratory model or of the prototype. In this paper we shall only check the theory against an experimental setup in a laboratory flume of fixed dimensions. To reduce the degree of empiricism, we determine the damping coefficients from a number of free oscillation tests, whereby the gates are released from some initial displacement consistent with the mode under study, without incident waves. The resulting coefficients will be used for predictions for wave-forced motions, which will then be compared with wave-forced experiments.

As a basis for such an exercise, we first solve (9.2) without the forcing term $c_F\left(A'/b'\right)\theta'^*$ and the detuning term $\left(\Delta\omega/\omega_0\right)\theta'$. In polar coordinates $\theta' = \mathscr{R}\mathrm{e}^{\mathrm{i}\psi}$, the resulting amplitude equation in $\mathscr{R}$ is simply

$$\mathscr{R}_{t'} = -\omega_0\mathscr{R}\left(c_R\mathscr{R}^2 + c_Q\mathscr{R} + c_L\right), \tag{9.3}$$

which can be solved in implicit form. Specifically the solution is

$$t' = \frac{1}{2c_L\omega_0}\left\{\log\left[\frac{c_R + c_L\mathscr{R}^{-2} + c_Q\mathscr{R}^{-1}}{c_R + c_L\mathscr{R}_0^{-2} + c_Q\mathscr{R}_0^{-1}}\right]\right.$$
$$\left. + \frac{1}{\mathscr{C}}\log\left[\frac{2c_R\mathscr{R} + c_Q\left(\mathscr{R}/\mathscr{R}_0 + 1\right) + 2c_L\mathscr{R}_0^{-1} + \mathscr{C}\left(\mathscr{R}/\mathscr{R}_0 - 1\right)}{2c_R\mathscr{R} + c_Q\left(\mathscr{R}/\mathscr{R}_0 + 1\right) + 2c_L\mathscr{R}_0^{-1} - \mathscr{C}\left(\mathscr{R}/\mathscr{R}_0 - 1\right)}\right]\right\} \tag{9.4a}$$

for $4c_Rc_L/c_Q^2 < 1$ where for brevity $\mathscr{C} = \left(1 - 4c_Rc_L/c_Q^2\right)^{1/2}$, and

$$t' = \frac{1}{2c_L\omega_0}\left\{\log\left[\frac{c_R + c_L\mathscr{R}^{-2} + c_Q\mathscr{R}^{-1}}{c_R + c_L\mathscr{R}_0^{-2} + c_Q\mathscr{R}_0^{-1}}\right] + \frac{2}{\mathscr{C}}\mathrm{atan}\left[\frac{\mathscr{C}(\mathscr{R} - \mathscr{R}_0)}{2c_L + 2c_R\mathscr{R}\mathscr{R}_0 + c_Q(\mathscr{R} + \mathscr{R}_0)}\right]\right\}, \tag{9.4b}$$

for $4c_Rc_L/c_Q^2 > 1$, with $\mathscr{C} = \left(4c_Rc_L/c_Q^2 - 1\right)^{1/2}$. $\mathscr{R} = \mathscr{R}_0$ is the initial value of $\mathscr{R}$ at $t' = 0$.

The laboratory flume is 0.38 m wide, 24 m long and 0.6 m high. A piston wavemaker is at one end and an absorbing beach composed of rubberized fibre mats at the other (figure 4*a*). Two hollow gates of Plexiglas walls, padded with styrofoam for added buoyancy, are hinged along a common axis across the flume at a central station, as shown in figure 4(*b*). The top of the box is connected through two aluminium rods to a potentiometer for measuring gate rotation. The distance d' of the centre of mass from the centre of rotation is measured by a strain gage. The inertia I' is evaluated from the period of the small-amplitude oscillations in air of the gate hanging upside down. In table 1 the essential features of the experimental setup are summarized. For this setup the non-dimensional eigenfrequency is calculated to be $G = 1.305$, which corresponds to a frequency of $\omega_0/2\pi = 0.713$ Hz. Next the following coefficients are calculated theoretically:

$$c_N = 2.49,\ c_R = 1.47,\ c_F = 0.90. \tag{9.5}$$

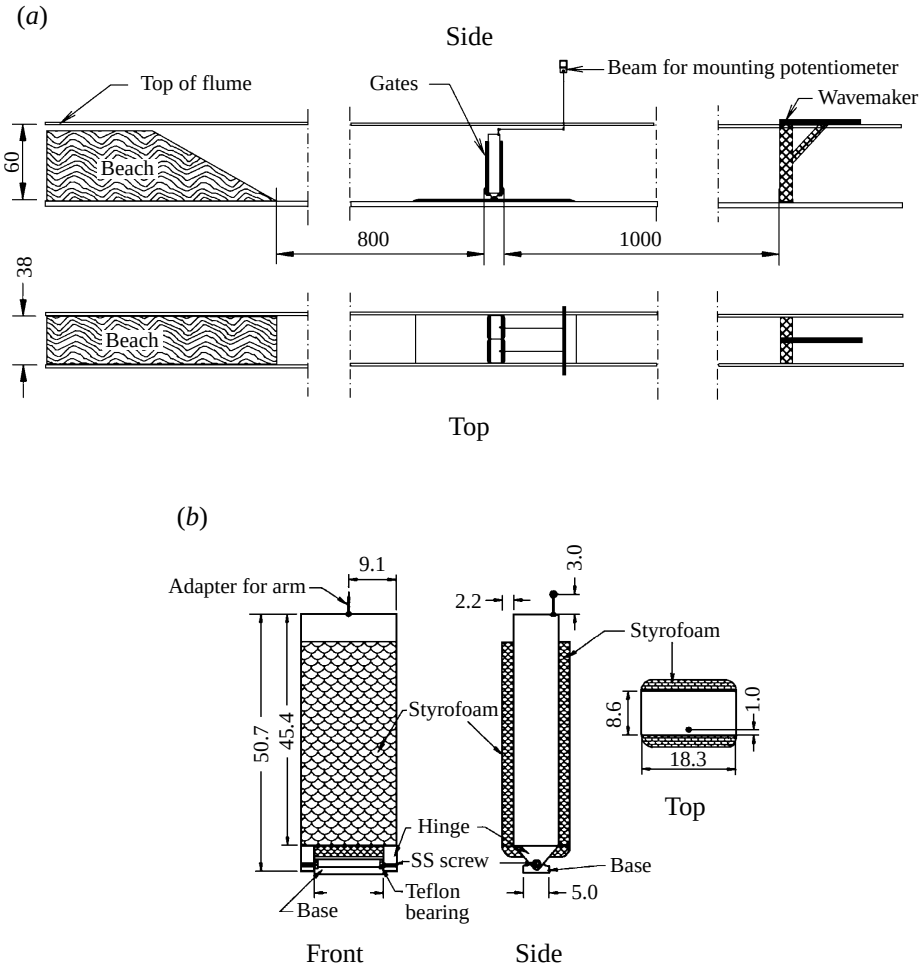

FIGURE 4. (*a*) Sketch of the wave flume. (*b*) Sketch of the gates used in the flume model. Dimensions in cm.

Time series records of the gate rotation are taken for several out-of-phase initial displacements, ranging from 4 deg to 10 deg. The best-fit values of c_L and c_Q are decided according to the following procedure. From a total of M experiments, $m = 1, \ldots, M$, we extract the $N(m)$ peak amplitudes from the time series $\{t'^{(e)}, \mathscr{R}^{(e)}\}_n$, $n = 1, \ldots, N(m)$. For each peak we calculate the squares of the difference between measured and the corresponding theoretical value according to (9.4*a*) and (9.4*b*). To get the best values of (c_L, c_Q) we minimize the sum of square errors at all peaks in all time series,

$$E(c_L, c_Q) = \sum_{m=1}^{M} \sum_{n=1}^{N(m)} \left(\mathscr{R}^{(e)} - \mathscr{R}\right)_n^2. \tag{9.6}$$

The results are

$$c_L = 0.009, \qquad c_Q = 0.291. \tag{9.7}$$

With these best-fit coefficients, the formulas (9.4*a*) and (9.4*b*) then agree with each individual time series of free oscillations very well. The fact that the same pair of

Dimensional data	Non-dimensional data
$I' = 0.106$ Kg m^2	$I = 0.014$
$M' = 1.271$ Kg	$M = 0.023$
$d' = 0.232$ m	$d = 0.617$
$S' = M'd' = 0.295$ Kg m	$S = Md = 0.014$
$a' = 0.070$ m	$a = 0.187$
$h' = 0.370$ m	$h = 0.992$
$b' = 0.376$ m	$b = 1.000$
$\rho = 1.004$ Mg m^{-3}	

TABLE 1. Geometrical and inertial parameters of the channel experiments

constants fits all records must be due to the narrow range of motion amplitudes. In prototype, the damping coefficients are unlikely to be constants and must be functions of motion and the gate geometry.

10. Theoretical results for uniform incident waves

We first summarize the theoretical results on equilibrium resonance (fixed points) and the instability. To simplify subsequent analysis we renormalize the variables as follows:

$$\left.\begin{aligned} &\alpha = \frac{c_R}{c_N}, \qquad \beta = \frac{c_L}{c_F A'/b'}, \qquad \gamma = \frac{c_Q}{\left(c_N c_F A'/b'\right)^{1/2}}, \\ &W = \frac{\Delta\omega/\omega_0}{c_F A'/b'}, \qquad \vartheta = \left(\frac{c_N}{c_F}\right)^{1/2} \frac{\theta'}{\left(A'/b'\right)^{1/2}}, \qquad T = c_F \frac{A'}{b'}\omega_0 t'. \end{aligned}\right\} \tag{10.1}$$

The evolution equation (9.2) becomes

$$-\mathrm{i}\vartheta_T = W\vartheta + (1+\mathrm{i}\alpha)\,\vartheta^2\vartheta^* + \vartheta^* + (1+\mathrm{i})\,\beta\vartheta + \mathrm{i}\gamma|\vartheta|\vartheta. \tag{10.2}$$

In this equation, W measures the frequency detuning between the incident wave and the eigenfrequency, α the radiation damping, β the linear viscous damping and γ the quadratic damping. Note that α is independent of A'/b', unlike β and γ.

Using action-angle variables R and ψ defined by $\vartheta = \mathrm{i}R^{1/2}\mathrm{e}^{\mathrm{i}\psi}$, we obtain from (10.2) an equivalent dynamical system in R and ψ

$$R_T = -2R\left(\alpha R + \sin 2\psi + \beta + \gamma R^{1/2}\right) \tag{10.3a}$$

$$\psi_T = W + R + \beta - \cos 2\psi. \tag{10.3b}$$

System (10.3b) admits at most three fixed points. In particular, the trivial fixed point is at $R = 0, \psi = (1/2)\cos^{-1}(W+\beta)$. By linearizing (10.3$a$) it is easy to show that the trivial fixed point is unstable for $|W+\beta| < \left(1-\beta^2\right)^{1/2}$, and stable otherwise. Note that in order for the region of instability to exist, the linear damping coefficient must satisfy $\beta < 1$. Using the definition (10.1) for β, it follows that for a given linear damping coefficient c_L, resonance from rest occurs only if A'/b' is larger than a threshold

$$\frac{A'}{b'} > \frac{c_L}{c_F} \tag{10.4}$$

as found by Miles (1990). Clearly this result is independent of the nonlinear damping terms.

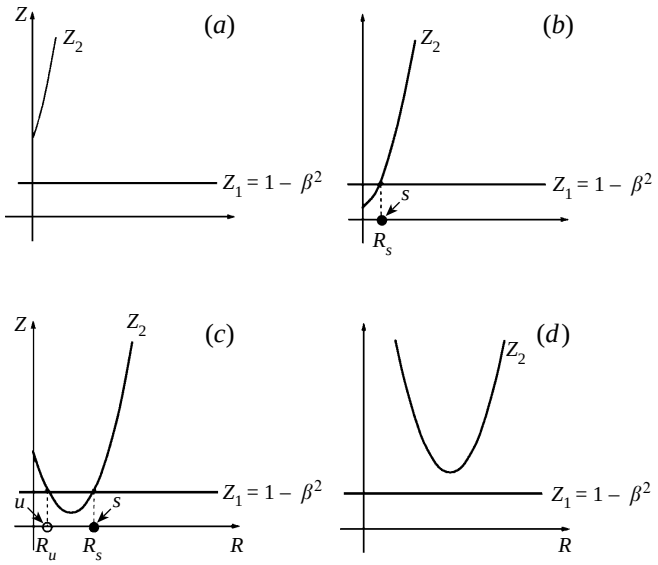

FIGURE 5. Graphical determination of the non-trivial fixed points and their stability. (*a*) For $W > \left(1-\beta^2\right)^{1/2} - \beta$ there are no intersections of Z_1 and Z_2; (*b*) for $|W+\beta| < \left(1-\beta^2\right)^{1/2}$ there is one intersection; (*c*) two intersections for $W_s < W < -\left(1-\beta^2\right)^{1/2} - \beta$; (*d*) no intersections for $W < W_s$.

There are also non-trivial fixed points with finite amplitude, corresponding to the roots of the algebraic equation

$$\left(1+\alpha^2\right) R^2 + 2\alpha\gamma R^{3/2} + \left(2W + 2\beta + 2\alpha\beta + \gamma^2\right) R + 2\beta\gamma R^{1/2} + (W+\beta)^2 = 1-\beta^2, \tag{10.5}$$

which can be solved numerically. Here we apply a graphical approach.

Corresponding to the two sides of (10.5), we consider the two curves

$$Z_1 = 1 - \beta^2 \tag{10.6}$$

and

$$Z_2 = \left(1+\alpha^2\right) R^2 + 2\alpha\gamma R^{3/2} + \left(2W + 2\beta + 2\alpha\beta + \gamma^2\right) R + 2\beta\gamma R^{1/2} + (W+\beta)^2 \tag{10.7}$$

in the auxiliary Z vs. R plane as in figure 5. The intersection(s) of the Z_1 and Z_2 curves is(are) the desired fixed point(s). Z_2 intersects the Z-axis at $Z = (W+\beta)^2$. Therefore, for $W > \left(1-\beta^2\right)^{1/2} - \beta$, Z_2 has no intersections with Z_1, as can be seen in figure 5(*a*). In the interval $|W+\beta| < \left(1-\beta^2\right)^{1/2}$ there is one intersection at $R = R_s$ and the corresponding fixed point will be labelled by s, as shown in figure 5(*b*). In the interval $W_s < W < -\left(1-\beta^2\right)^{1/2} - \beta$, there are two intersections at $R = R_s$ and $R = R_u$ (corresponding to fixed points s and u respectively), shown in figure 5(*c*). The two intersections coalesce when $W = W_s$, i.e. when Z_2 is tangent to Z_1, corresponding to a saddle-node bifurcation. Finally for $W < W_s$ no intersections are possible since Z_2 lies above Z_1 (see figure 5*d*). The conditions for a tangent intersection are

$$Z_2 = Z_1 \qquad \frac{\mathrm{d}Z_2}{\mathrm{d}R} = 0 \tag{10.8}$$

which can only be solved numerically for W_s and R.

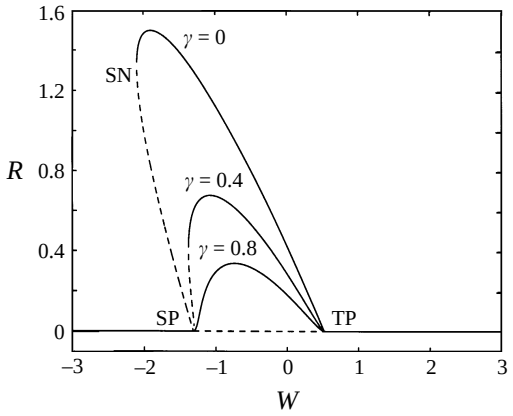

FIGURE 6. Bifurcation diagram for different values of quadratic viscous damping γ. The larger γ the smaller the stable fixed point action; the bandwidth of instability is not affected by γ.

The Jacobian at the non-trivial fixed points (s,u) is

$$\boldsymbol{J} = \begin{bmatrix} -2\alpha R - \gamma R^{1/2} & -4R(W+\beta+R) \\ 1 & -2\alpha R - 2\gamma R - 2\beta \end{bmatrix}, \tag{10.9}$$

where R now represents the action of s or u (i.e. R_s or R_u). The eigenvalues of the Jacobian are given by

$$-2\alpha R - \beta - \tfrac{3}{2}\gamma R^{1/2} \pm \left[-4R(W+\beta+R) + \beta^2 + \beta\gamma R^{1/2} + \tfrac{1}{4}\gamma^2 R\right]^{1/2}. \tag{10.10}$$

The fixed point is unstable if and only if the larger eigenvalue is positive, i.e. if

$$-2R\left\{2\left(1+\alpha^2\right)R + 3\alpha\gamma R^{1/2} + \beta\gamma R^{-1/2} + 2W + 2\beta + 2\alpha\beta + \gamma^2\right\} \equiv -2R\left\{\frac{\mathrm{d}Z_2}{\mathrm{d}R}\right\} > 0. \tag{10.11}$$

Since $R > 0$ by definition, the fixed point is unstable if

$$\frac{\mathrm{d}Z_2}{\mathrm{d}R} < 0 \tag{10.12}$$

at the point of intersection of Z_2 and Z_1. We conclude from figures 5(b) and 5(c) that, if existing, s is always stable while u is always unstable, hence the notation.

The solution of (10.5) for R as a function of W gives the bifurcation diagram shown in figure 6 for $\alpha = \beta = 0.4$ and for a range of γ. By taking

$$\frac{\mathrm{d}}{\mathrm{d}W}(10.5) = 0, \tag{10.13}$$

the maximum amplitude of s is found at $W = -R_{s_{max}} - \beta$, with the value

$$R_{s_{max}} = \frac{1-\beta}{\alpha} - \frac{\gamma^2}{2\alpha^2}\left\{\left[1 + \frac{4\alpha}{\gamma^2}(1-\beta)\right]^{1/2} - 1\right\}, \tag{10.14}$$

which is the maximum of the stable response. Clearly as γ increases, R_s decreases. For $\gamma = 0.0$ and 0.4, u corresponds to the dashed curve in figure 6 going from the subcritical pitchfork (SP) to the saddle node (SN) bifurcation. Note that γ does not alter the region of linearized instability. However, an increase in γ moves the saddle node SN toward $W = 0$ therefore reducing the parametric region of hysteresis. Beyond

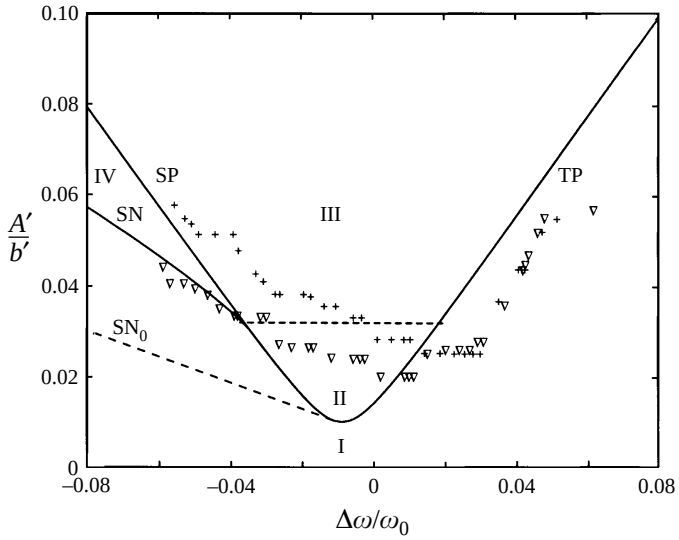

FIGURE 7. The regions of instability and hysteresis in the plane of $\Delta\omega/\omega_0$ vs. A'/b'. Region I: stable trivial fixed point. Regions II and III: unstable trivial fixed point coexisting with s (region of instability). Region IV: stable trivial fixed point coexisting with s and u (region of hysteresis).

a certain threshold γ, u disappears and the saddle-node bifurcation does not occur. In this case s is born as a transcritical bifurcation at both $W = \pm\left(1-\beta^2\right)^{1/2} - \beta$ (see the curve for $\gamma = 0.8$) and hysteresis does not occur.

It is physically revealing to display the region of instability in the $\Delta\omega/\omega_0$ vs. A'/b' plane (see figure 7). Using the definition (10.1) of β and W, the threshold of instability of the trivial fixed point, i.e. the resonance of the trapped mode, $W = \pm\left(1-\beta^2\right)^{1/2} - \beta$ is mapped onto the hyperbola in the plane of $\Delta\omega/\omega_0$ vs. A'/b':

$$\frac{\Delta\omega}{\omega_0} = \pm\left[c_F^2\left(\frac{A'}{b'}\right)^2 - c_L^2\right]^{1/2} - c_L. \tag{10.15}$$

The vertex of the hyperbola lies at

$$\frac{\Delta\omega}{\omega_0} = -c_L, \qquad \frac{A'}{b'} = \frac{c_L}{c_F}, \tag{10.16}$$

which corresponds to marginal instability $W = -\beta$, $\beta = 1$ and the existence of the non-trivial root s. In figure 7 the hyperbola (10.15) is plotted for the gate and channel characteristics of our experiments in the wave channel, as will be described shortly. Along the + branch of (10.15), denoted by TP in figure 7, the origin loses stability in a transcritical pitchfork bifurcation. Along the − branch, denoted by SP, the origin loses stability in a subcritical pitchfork bifurcation (compare with the points TP and SP of figure 6). The region above the hyperbola (the union of II and III in figure 7) corresponds to instability, where a finite-amplitude trapped wave will be resonated. Note that the larger is c_F, the lower is the instability threshold and the larger is the region of instability. The dependence of c_F on the gate characteristics and water depth will be discussed next.

By using (10.1), the condition for a saddle-node bifurcation, $W = W_s$ (obtained by numerical solution of (10.8)), can be mapped onto a line in the plane of $\Delta\omega/\omega_0$

vs. $\overline{A}'/b'$, marked by SN in figure 7. This line is tangent to the $-$ branch SP of the hyperbola (10.15).

The horizontal dashed line passing the point of tangency of SN and SP separates the region of instability in two sub-regions II and III. In II if we fix the amplitude A' and vary $\Delta\omega$, the bifurcation curve is similar to the curve of figure 6 marked by $\gamma = 0.8$, i.e. the non-trivial solution s starts and ends at $R = 0$ with two transcritical pitchfork bifurcations. Therefore more properly the curve TP is the union of the $+$ branch of the hyperbola and the part of the $-$ branch from the vertex to the point of tangency with SN. On the other hand, in region III, the bifurcation diagram is similar to the curves figure 6 marked by $\gamma = 0.0$ or 0.4, i.e. at SP the value of s is non-zero and extends continuously in the hysteresis interval. The interval of hysteresis $W \in \left[W_s, -\left(1-\beta^2\right)^{1/2} - \beta\right]$ of figure 6, is mapped onto region IV delimited by SP and SN in the $\Delta\omega/\omega_0$ vs. A'/b' plane.

If quadratic viscous damping is ignored, $\gamma = 0$, the tangency condition has an explicit expression (Miles 1990)

$$W_s = \frac{\beta}{\alpha} - \left(1 + \frac{1}{\alpha^2}\right)^{1/2} - \beta, \tag{10.17}$$

which in terms of the physical variables can be written as

$$\left(\frac{\Delta\omega}{\omega_0}\right)_s = c_L \frac{c_N}{c_R} - \left[1 + \left(\frac{c_N}{c_R}\right)^2\right]^{1/2} c_F \frac{A'}{b'} - c_L, \tag{10.18}$$

and is represented by a long-dashed straight line in figure 7 denoted by SN_0.

11. Effects of gate and channel characteristics on steady resonance

The frequency bandwidth of instability is of engineering interest for it represents the frequency range in which the resonance phenomenon occurs. From (10.15), the asymptotes of the hyperbola bounding the region of instability form a wedge with the sides given by the straight lines

$$\frac{\Delta\omega}{\omega_0} = \pm c_F \frac{A'}{b'} - c_L. \tag{11.1}$$

Thus the apex of the wedge is at $\Delta\omega/\omega_0 = -c_L$ and c_F is a measure of the opening of the hyperbola (10.15), i.e. for a given incident wave A', a larger c_F gives a wider band of instability.

From equation (10.18) we see that for larger c_N, the line SN_0 is less inclined, resulting in a larger region of hysteresis (see figure 7), i.e. c_N is also a measure of the tilt of the resonance response curve towards negative detuning. The effect of c_Q is to counteract the effect of c_N, i.e. the quadratic dissipation coefficient changes SN_0 to SN making the region of hysteresis smaller.

As a crude guide for the effects of gate characteristics on the *maximum equilibrium amplitudes* of gate oscillations at full resonance, we ignore frictional damping by setting $\beta = \gamma = 0$ in (10.14), thus

$$R_{s_{max}} = \frac{1}{\alpha}. \tag{11.2}$$

Using physical variables (11.2) becomes

$$|\theta'|_{max} = \left(\frac{c_F}{c_R}\frac{A'}{b'}\right)^{1/2}. \tag{11.3}$$

Thus for a given incident wave A', the maximum equilibrium amplitude is smaller for smaller $\left(c_F/c_R\right)^{1/2}$. We may therefore refer to $\left(c_F/c_R\right)^{1/2}$ as the (inviscid) amplification factor: it represents the result of the balance between the forcing by the incident wave, c_F, and the radiation damping, c_R. Recall from (10.14) that in the same inviscid limit, the maximum value occurs for negative detuning at

$$W = -R_{s_{max}} = -\frac{1}{\alpha}, \tag{11.4}$$

or in physical variables

$$\frac{\Delta\omega}{\omega_0} = -c_N\frac{c_F}{c_R}\frac{A'}{b'}, \tag{11.5}$$

hence an increase in c_N moves the frequency of the maximum value towards negative detuning, confirming the fact that the magnitude of c_N affects the tilting of the resonance curve towards negative detuning.

We now discuss the dependencies of c_F (bandwidth of instability) and of the ratio $\left(c_F/c_R\right)^{1/2}$ (amplification factor) on the gate and channel properties. As in §6 for G, we consider for simplicity homogeneous gates of density ρ_g.

In figures 3(d) and 8 the water depth is fixed, $h = 1$; the first and second moments of inertia S, I, with $S = 0.65I$, are increased from zero, by increasing ρ_g. Different values of gate thickness a are examined: 0.10, 0.20, 0.30. As the inertia increases, the bandwidth of instability decreases. For a fixed inertia (fixed abscissa in figure 3d), an increase in a induces an increase in the bandwidth of instability.

The amplification factor versus the inertia I, also for $S = 0.65I$, is plotted in figure 8. The variation is similar to that of G of figure 2. For $I \to 0$ the amplification factor approaches a finite value. For increasing value of the inertia, the factor also increases and becomes unbounded as $S \to ah^2/2$. Therefore, for heavier gates, not only is the natural period longer, but the resonant response is also larger. Thus heavier gates oscillate slower and with larger amplitude! However, the likelihood of resonance is reduced because of the smaller bandwidth of instability. For any fixed value of the gate inertia (fixed abscissa in figure 8), an increase in a reduces the response.

We have also fixed the thickness a and varied $S = \alpha I$ for different water depth h. As can be found in Sammarco (1996) the trend is the same as in figures 3(d) and 8 for fixed h. The bandwidth of instability decreases with increasing I and with decreasing h. On the other hand, the amplification factor increases with increasing I and decreases for increasing water depth h (the larger the displaced volume ah, the smaller the response).

Therefore, to maximize resonance in a laboratory experiment, the gate should have small inertia and large buoyancy ah. To minimize resonance in the prototype is a more delicate matter, however, since a smaller response is associated with larger instability bandwidth. A suitable design must be made by considering the spectral shape of the incident sea.

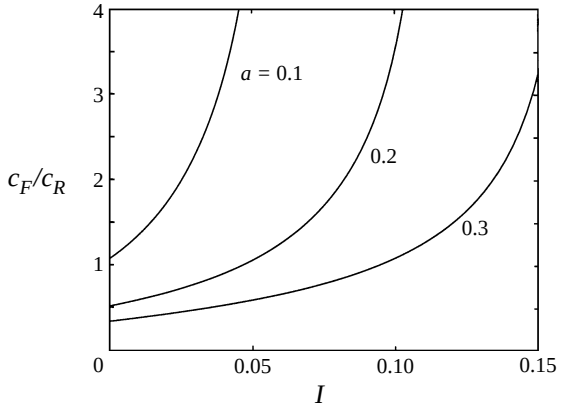

FIGURE 8. Amplification factor for $h = 1$ and varying $S = 0.65I$; $a = 0.1$, 0.2 and 0.3.

12. Comparison with experiments in a wave channel

To verify these predictions, we have performed experiments with two vertical gates in a wave flume; the set-up was described in §9. Extensive tests for a range of incident wave amplitudes and frequencies slightly detuned from twice the natural frequency $2\,(\omega_0/2\pi) = 1.426$ Hz are made. Because of the finite flume length, waves reflected by the gates are reflected again by the wave-making pistons. To account for this re-reflection we take wave records from two wave gauges separated by a fixed distance along the centreline of the flume, on each side of the gates. From the recorded spectra at two gates on the incidence side, the amplitudes of the incident and reflected waves can be calculated. Similar records on the reflection side gives the reflection coefficient, which is found to lie between 1% and 7% in the range of frequency tested (1.0 to 1.5 Hz). With the help of computer automation, two series of tests are performed. In the first, almost continuous scanning of incident wave amplitude is made for several chosen frequencies; while in the second, almost continuous scanning of wave frequency is made for several chosen wave amplitudes. Referring to the instability diagram figure 7, we start from the regime of stability. Each incident amplitude is kept steady for at least 150 s, and then increased by a small increment of 0.001 m without stopping the motor. The upward scan is terminated at some maximum amplitude beyond the instability threshold. The typical range of incident wave amplitude A' is from 0.009 m to 0.025 m. The scanning process is then reversed by reducing the amplitude from the unstable to the stable region. These two-way amplitude scans are repeated for several frequencies.

In a frequency scan, the wave amplitude is kept fixed; the frequency is varied quasi-statically downward from a positive detuning outside the instability region, through the instability and the hysteresis regions, and finally down to negative detuning. The same range is then scanned upward from negative to positive detuning.

The threshold of instability is shown in figure 7. For each amplitude scan, the threshold amplitudes are defined by the condition that the associated gate response at half the incident wave frequency is 0.10°†. Distinctions are made between thresholds in an upward amplitude scan (crosses) a downward amplitude scan (triangles). Similarly,

† Theoretically the threshold should correspond to zero gate amplitude.

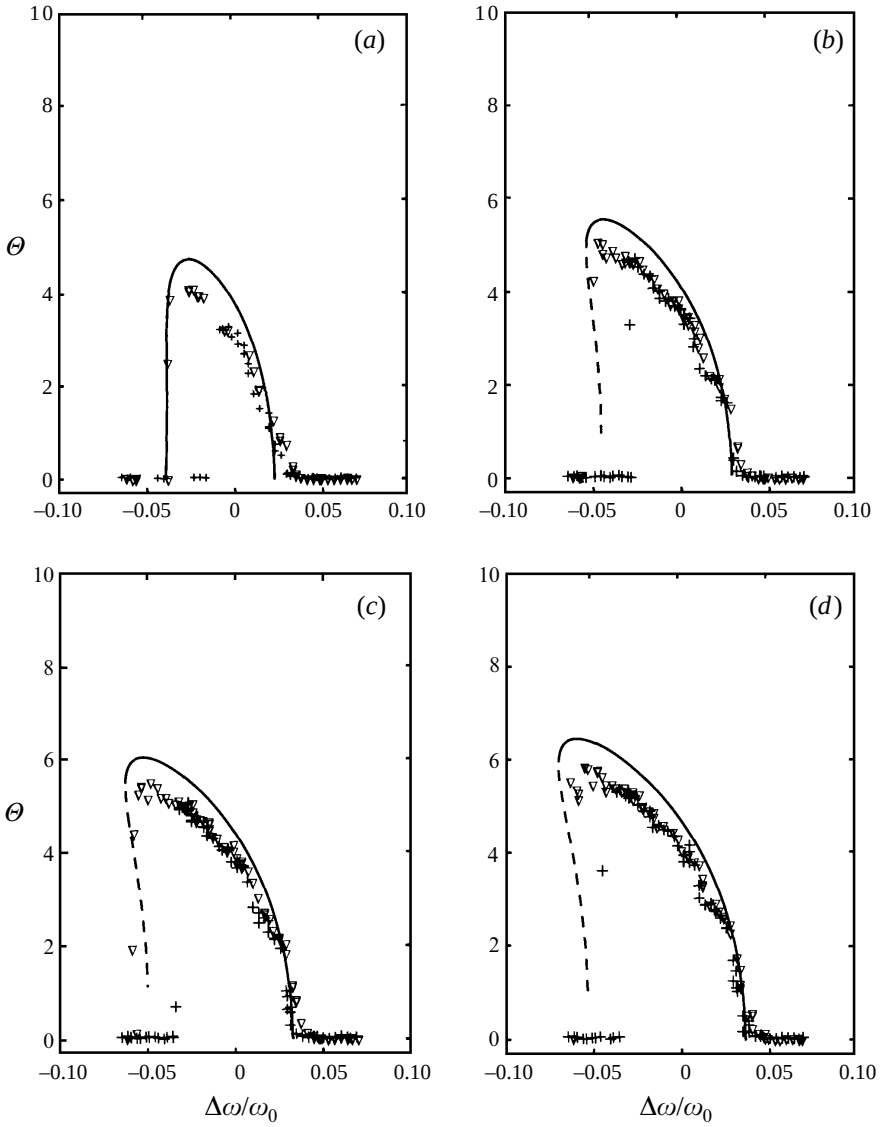

FIGURE 9. Frequency scans: theory vs. experiments. Θ is in degrees. (*a*) $A'/b' = 0.035$; (*b*) $A'/b' = 0.043$; (*c*) $A'/b' = 0.047$; (*d*) $A'/b' = 0.051$.

for each frequency scan, the threshold frequencies are defined by the condition that the subharmonic gate response is 0.10°. Again crosses denote the results for upward scans and triangles for downward scans. The resulting data from the two type of scans are plotted together in figure 7. Clearly the existence of two different thresholds at negative detuning is a partial confirmation of the hysteresis phenomenon. Quantitative agreement on the threshold of instability is not totally satisfactory, owing probably to the difficulty in defining the threshold of zero growth rate and the limited duration of each time series.

Sample measured equilibrium gate amplitudes are plotted in the frequency and amplitude scans of figure 9 and figure 10 respectively. Again crosses denote up-

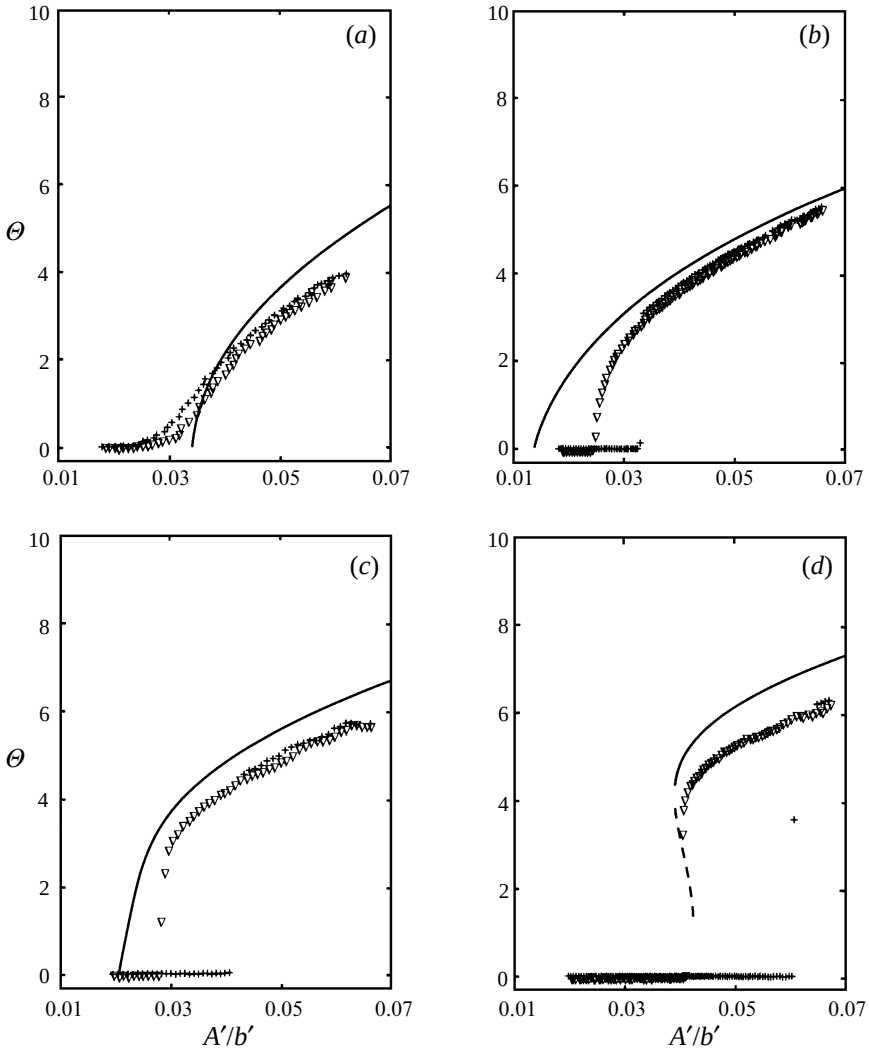

FIGURE 10. Frequency scans: theory vs. experiments. Θ is in degrees. (*a*) $\Delta\omega/\omega_0 = 0.020$; (*b*) $\Delta\omega/\omega_0 = -0.003$; (*c*) $\Delta\omega/\omega_0 = -0.023$; (*d*) $\Delta\omega/\omega_0 = -0.044$.

ward scans, triangles downward scans. Figure 9 shows four different frequency scans for respectively $A'/b' = 0.035$, 0.043, 0.047 and 0.051. Figure 10 shows four different amplitude scans at respectively $\Delta\omega/\omega_0 = 0.020$, -0.003, -0.023 and -0.044. Clearly the feature of hysteresis is further confirmed. The agreement is much better at higher incident wave amplitudes, consistent with the fact that higher accuracy in measurement is easier to achieve at higher amplitudes. Given the fact that the empirical damping coefficients are obtained only from free gate oscillations without incident waves, the corroboration signifies the essential correctness of the theory.

Theoretically the equilibrium gate amplitude Θ, the incident wave amplitude A'/b' and frequency $\Delta\omega/\omega_0$ form the bifurcation surface in the three-dimensional parameter space. The fact that data from the upward (or downward) scans fall on the same surface not only provides a check of the consistency of experiments, but also

reconstructs the predicted bifurcation surface corresponding to the phenomenon of hysteresis.

13. Conclusions

Extending the linear theory of Mei *et al.* (1994), we have derived the nonlinear evolution equation for the out-of-phase oscillation of Venice gates. The theory is similar in principle to the parametric subharmonic resonance of edge waves on a beach, but considerable analysis is required to calculate the coefficients of the Landau–Stuart equation in terms of the gate dimensions and water depth. To reduce computations, the gates are assumed to be upright when in equilibrium.

We have shown that gates with larger inertia have smaller eigenfrequency, i.e. heavier gates oscillate slower. For fixed gate inertia, an increase in the displaced volume induces an increase in the eigenfrequency. The effect of increasing gate width is to decrease the eigenfrequency. Finally, for fixed gate characteristics, deeper water is accompanied by higher natural frequencies. To avoid unwanted resonances, a solution is to decrease the natural frequency below the range of the local incident wave frequencies, either by decreasing the displaced volume or by increasing the gate inertia and/or gate width. Another solution is to render the gates so buoyant that their natural frequency is far higher than the above incident sea spectrum. However an articulated gate array has other natural modes at lower frequencies, which may still be excited by the incident wave.

Knowledge of the coefficients of the Landau–Stuart equation has allowed us to predict the threshold and the frequency bandwidth of instability, and the equilibrium amplitude of the resonated mode. We have shown that, once resonated, heavier gates oscillate slower and with larger amplitude. For a fixed inertia, an increase of gate displacement induces a decrease in the resonant response. A similar effect can be achieved by an increase of water depth. As the gate inertia increases, the response increases, but the bandwidth of unstable frequencies decreases. Thus heavier gates are increasingly more difficult to excite, though the resonance response may be larger.

A detailed comparison with laboratory experiments have been made to confirm theoretical predictions for uniform incident waves. After adding viscous terms with damping coefficients determined only from free oscillations, all important theoretical predictions are corroborated by experiments with a uniform incident waves. In particular the jump phenomenon associated with the hysteretic amplitude–frequency relation is confirmed for the first time. Thus the Landau–Stuart equation, which is important in many modern problems of nonlinear phenomena, is found to play a role in breakwater engineering, an endeavour already practised by Egyptians thousands of years ago, for the harbour of Alexandria.

In this work, possible long-scale variation in the y-direction along the barrier has not been investigated. Such non-uniformity should be governed by the cubic Schrödinger equation and deserves further study.

We thank Professor Alberto Noli, University of Rome, and Professor Attilio Adami, University of Padua, for their encouragement which initiated the authors' interests in this problem. Mr Carlo Procaccini took part in the early phase of the experiments. Funding has been provided by grants from US Office of Naval Research (Accelerated Research Initiative on Nonlinear Ocean Waves directed by Dr. Thomas Swean (Grant N00014-92-J-1754, and N00014-95-1-8040 (AASERT)), US National Science Foun-

dation (Grants CTS-9115689 and CTS-9634120) directed by Drs Stephen Traugott and Roger Arndt, and Consorzio Venzia Nuova for laboratory equipments.

Appendix. The second-order, second harmonic

The second harmonic is forced by an incident plane wave from $x \sim \infty$ and by the trapped wave through quadratic nonlinearities. Both types of forcing oscillate at twice the natural frequency.

A.1. *Response to nonlinear forcing: a radiation problem*

In view of equations (6.6) and (6.7), θ^2 can be factored from the forcing terms of the second harmonic leaving only the real coefficients $f_{11}^{\pm}$ and q_{11}, so that

$$\mathscr{F}_{22}^{\pm} = \mathrm{i}\theta^2 \left(-\frac{3}{G^2} f_{11}^{\pm^2} + f_{11}^{\pm} f_{11_{zz}}^{\pm} - 2 f_{11_x}^{\pm^2} - 2 f_{11_y}^{\pm^2} \right)_{z=0}, \tag{A 1}$$

$$\mathscr{B}_{22}^{\pm} = -2\mathrm{i}\phi_{22}^{\pm} - \theta^2 \left(\frac{1}{G} f_{11_z}^{\pm} f_{11}^{\pm} + \tfrac{1}{2} |\nabla f_{11}^{\pm}|^2 \right), \tag{A 2}$$

$$\mathscr{G}_{22}^{\pm} = \pm \mathrm{i}\theta^2 \left[-(z+h) f_{11_{xx}}^{\pm} q_{11} + f_{11_z}^{\pm} q_{11} - a q_{11}^2 \right], \tag{A 3}$$

$$\mathscr{D}_{22} = 0. \tag{A 4}$$

The forcing term $\mathscr{D}_{22}$ vanishes because the symmetry properties (6.12) annihilate all the differences $\Delta(\cdot)$, $\Delta_0(\cdot)$ and the averages $\overline{(\cdot)}$ across the two sides of the gate. Because each of the quadratic products is an even periodic function of y, so are the forcing terms $\mathscr{F}_{22}^{\pm}$ and $\mathscr{G}_{22}^{\pm}$. Therefore $\mathscr{F}_{22}^{\pm}$ and $\mathscr{G}_{22}^{\pm}$ can also be expanded in Fourier cosine series:

$$\mathscr{F}_{22}^{\pm} = \mathrm{i}\theta^2 \sum_{p=0}^{\infty} \Gamma_p^{\pm}(x) \cos p\pi y, \quad \mathscr{G}_{22}^{\pm} = \pm \mathrm{i}\theta^2 \sum_{p=0}^{\infty} \Lambda_p^{\pm}(z) \cos p\pi y. \tag{A 5}$$

Because of the form of the forcing terms, (A 5), the velocity potential and the gate rotation can be split into two parts as in (7.7). The conditions governing $f_{22}^{\pm}(x, y, z)$ can be derived from (5.19)–(5.24), yielding the following boundary value problem:

$$\nabla^2 f_{22}^{\pm} = 0 \qquad \text{in} \quad \Omega^{\pm}, \tag{A 6}$$

$$G f_{22_z}^{\pm} - 4 f_{22} = \sum_{p=0}^{\infty} \Gamma_p^{\pm}(x) \cos p\pi y, \qquad z = 0, \tag{A 7}$$

$$f_{22_z}^{\pm} = 0, \qquad z = -h, \tag{A 8}$$

$$f_{22_x}^{\pm} - 2(z+h) q_{22} = \pm \sum_{p=0}^{\infty} \Lambda_p(z) \cos p\pi y, \qquad x = 0, \tag{A 9}$$

$$-4I q_{22} + GC q_{22} = \mathrm{i}2 \int_{y_1}^{y_2} \mathrm{d}y \int_{-h}^{0} \mathrm{d}z \, \{ f_{22}(z+h) \}, \qquad x = 0, \tag{A 10}$$

where

$$q_{22} = \begin{cases} q^I & \text{for} \quad 0 < y < 1/2 \\ q^{II} & \text{for} \quad 1/2 < y < 1. \end{cases} \tag{A 11}$$

Solution can be achieved by expanding $f_{22}^{\pm}$, q_{22} in Fourier series

$$f_{22}^{\pm} = \sum_{p=0}^{\infty} F_p^{\pm}(x,z)\cos p\pi y, \qquad q_{22} = \sum_{p=0}^{\infty} c_p \cos p\pi y. \tag{A 12}$$

The two-dimensional boundary value problem for each Fourier coefficient in (A 12) can be straightforwardly solved by the eigenfunction expansion method, subject to the radiation condition at $x \sim \pm\infty$.

A.2. *Scattering of incident waves*

This is a simple diffraction problem in two dimensions. Let the incident wave in the (x, z)-plane be

$$\eta_{22}^{I} = \tfrac{1}{2}A_2 \mathrm{e}^{-\mathrm{i}\kappa x} \tag{A 13}$$

and

$$\phi_{22}^{I} = -\frac{\mathrm{i}GA_2}{4}\frac{\cosh\kappa(z+h)}{\cosh\kappa h}\mathrm{e}^{-\mathrm{i}\kappa x}, \tag{A 14}$$

where κ is the real root of the dispersion relation:

$$4 = G\kappa\tanh\kappa h. \tag{A 15}$$

The scattered wave field $\phi_{22}^{(A)}$ is governed by the following boundary value problem:

$$\phi_{22_{xx}}^{\pm\,(A)} + \phi_{22_{zz}}^{\pm\,(A)} = 0 \quad \text{in} \quad \Omega^{\pm} \tag{A 16}$$

$$G\phi_{22_z}^{\pm\,(A)} - 4\phi_{22}^{\pm(A)} = 0, \quad z = 0, \tag{A 17}$$

$$\phi_{22_z}^{\pm\,(A)} = 0, \quad z = -h, \tag{A 18}$$

$$\phi_{22_x}^{+\,(A)} = 2\mathrm{i}(z+h)\theta_{22}{}^{(A)} - \phi_{22_x}^{I}, \quad x = 0^{+} \tag{A 19}$$

$$\phi_{22_x}^{-\,(A)} = 2\mathrm{i}(z+h)\theta_{22}{}^{(A)}, \quad x = 0^{-}, \tag{A 20}$$

and the radiation condition at $x \sim \pm\infty$. Coupling with the corresponding gate rotation $\theta_{22}^{(A)}$ is constrained by the equation of motion of the gate

$$-4I\theta_{22}^{(A)} + GC\theta_{22}^{(A)} = \mathrm{i}2\int_{y_1}^{y_2}\mathrm{d}y\int_{-h}^{0}\mathrm{d}z\left\{\left(\phi_{22}^{(A)} + \phi^{I}\right)(z+h)\right\}, \qquad x = 0. \tag{A 21}$$

The solution of (A 16)–(A 20) can be carried out in term of eigenfunction expansions.

REFERENCES

Blondeaux, P., Seminara, G. & Vittori, G. 1993*a* Linear response of the gate system for protection of the Venice Lagoon. Note I. Transverse free modes. *Rend. Mat. Acc. Lincei* A **59**, 291–298.

Blondeaux, P., Seminara, G. & Vittori, G. 1993*b* Linear response of the gate system for protection of the Venice Lagoon. Note II. Excitation of transverse subharmonic modes. *Rend. Mat. Acc. Lincei* A **59**, 299–305.

Buchan, S. J. & Pritchard, W. G. 1995 Experimental observations of edge waves. *J. Fluid Mech.* **288**, 1–36.

Consorzio "Venezia Nuova" 1988*a* Modelli fisici delle paratoie a spinta di galleggiamento (in Italian). *Tech. Rep. 291 Estramed SpA.*

Consorzio "Venezia Nuova" 1988*b* Study on the influence of the inclination angle and the gate shape on gate response. Studio 2.2.10. *Tech. Rep. Delft Hydraulics.*

Dore, B. D. 1969 The decay of oscillations of a non-homogeneous fluid within a container. *Proc. Camb. Phil. Soc.* **65**, 301–307.

Greenspan, H. P. 1968 *The Theory of Rotating Fluid*. Cambridge University Press.

Guza, R. T. & Bowen, A. J. 1976 Finite amplitude Stokes edge waves. *J. Mar. Res.* **34**, 269–293.

Henderson, D. M. & Miles, J. W. 1991 Faraday waves in 2:1 internal resonance. *J. Fluid Mech.* **222**, 449–470.

Jiang, L., Ting, C., Perlin, M. & Schultz, W. W. 1996 Moderate and steep Faraday waves instabilities, modulation and temporal asymmetries. *J. Fluid Mech.* **329**, 275–307.

Johns, B. 1968 A boundary layer method for the determination of the viscous damping of small amplitude gravity waves. *Q. J. Mech. Appl. Maths* **21**, 93–103.

Jongeling, T. H. G. & Kolkman, P. A. 1995 Subharmonic standing cross waves leading to low-frequency resonance of a submercible flap-gate barrier. *Proc. 6th Intl Conf. Flow-induced Vibrations, Imperial College, UK April 10–15*.

Mei, C. C. 1989 *The Applied Dynamics of Ocean Surface Waves*. World Scientific, Teaneck, NJ.

Mei, C. C. & Liu, X. 1973 The damping of surface gravity waves in a bounded liquid. *J. Fluid Mech.* **59**, 239–256.

Mei, C. C., Sammarco, P., Chan, E. S. & Procaccini, C. 1994 Subharmonic resonance of proposed storm gates for Venice Lagoon. *Proc. R. Soc. Lond.* A **444**, 463–479.

Miles, J. W. 1990 Parametrically excited standing edge waves. *J. Fluid Mech.* **214**, 43–57.

Miles, J. W. 1993 On Faraday waves. *J. Fluid Mech.* **248**, 671–683.

Minzoni, A. A. & Whitham, A. J. 1977 On the excitation of edge waves on beaches. *J. Fluid Mech.* **79**, 273–287.

Rockliff, N. 1978 Finite amplitude effects in free and forced edge waves. *Math. Proc. Camb. Phil. Soc.* **83**, 257–265.

Sammarco, P. 1996 Theory of subharmonic resonance of Venice Lagoon storm gates. PhD thesis, MIT, Dept. of Civil & Environmental Engineering.

Sammarco, P., Tran, H. H., Gottlieb, O. & Mei, C. C. 1997 Subharmonic resonance of Venice gates in waves. Part 2. Sinusoidally modulated incident waves. *J. Fluid Mech.* **349**, 327–359.

Tran, H. 1996 Experiments on subharmonic resonance of Venice Lagoon storm gates. MS thesis, MIT, Dept. of Civil & Environmental Engineering.

Varisco, D. 1992 Interaction between flap gates and tidal current and waves. *Abstract 23rd Conf. Coastal Engineering*, ASCE.

Vittori, G., Blondeaux, P. & Seminara G. 1996 Waves of finite amplitude trapped by oscillating gates *Proc. R. Soc. Lond.* A **452**, 791–811.